6 3 - 4 - 5

GD|C-63-132 A

EXPERIMENTAL INVESTIGATION OF SUPERCAVITATING HYDROFOIL FLUTTER PHENOMENA

AUGUST 1963

EXPERIMENTAL INVESTIGATION OF
SUPERCAVITATING HYDROFOIL FLUTTER PHENOMENA

Robert C. Peller
Louis M. Figueroa

FOREWORD

Considerable work in the field of the theory of supercavitating hydrofoils has been accomplished to date, but little experimental work has been done to verify the theories thus generated. The results presented in this report consider the flutter characteristics of a surface-piercing supercavitating hydrofoil with a rudder — or spoiler — type control surface.

This experimental work was carried out by General Dynamics/Convair under Navy Bureau of Ships Contract NObs-86810, Project Serial No. SF-013-02-01, Task 1719.

CONTENTS

ILLUSTRATIONS

ILLUSTRATIONS (Continued)

TABLES

NOMENCLATURE

b   =   semi-chord length

C_R =   chord of rudder

C_S =   chord of spoiler

F_n =   flexure design uncoupled natural frequencies:

<u>Rudder</u>

F_1 =   90 cps

F_2 =   55 cps

F_3 =   21 cps

<u>Spoiler</u>

F_1 =   300 cps

F_2 =   135 cps

F_3 =   30 cps

h   =   depth of immersion

1   =   length of foil

m   =   mass per unit length

R_n =   rudder model:

R_1 =   15 per cent chord (0.9 in.)

R_2 =   25 per cent chord (1.5 in.)

R_3 =   35 per cent chord (2.1 in.)

S_n = spoiler model:

S_1 = 5 per cent chord (0.30 in.)

S_2 = 7 per cent chord (0.42 in.)

S_3 = 10 per cent chord (0.60 in.)

V = foil velocity

μ = mass ratio = $m/\pi\rho b^2$

ρ = density

ψ = foil angle of attack

ω = frequency

1 | INTRODUCTION

The use of supercavitating hydrofoils can be advantageous, especially as speeds of hydrofoil boats are increased to speeds in excess of 60 knots. Supercavitation also can be of value in the design of pumps and machines intended to operate at very low pressures, as those required in the handling of cryogenic fluids. However, this has not always been the case and cavitation on propeller blades has led to very inefficient operation and erosion of the blades. Largely due to the work of Tulin, efficient supercavitating hydrofoil sections have been developed and are now of considerable use in pump and high-speed hydrofoil design.

One facet in the design of hydrofoils that must be evaluated before a satisfactory piece of hardware can be built is the hydrodynamic stability of the foils. Instabilities in this category are divergence and flutter which are functions of the stiffness, mass distribution and oscillatory loads on the foils. In the aircraft field, these investigations are carried out under the heading of aeroelasticity. Initial efforts at understanding these problems when applied to bodies in water were extensions of the aeroelastic theory and resulted in some inconsistencies largely due to the different viscous effects and to the low values of mass ratio at which the waterborne devices were operated. Thus, the new field of hydroelasticity came into being.

Considerable work has been accomplished, both theoretical and experimental, in the investigation of subcavitating, submerged and surface-piercing hydrofoils. However, supercavitating flow has not been investigated as thoroughly. Most of the work has been concentrated in the theoretical field with a comparatively small amount of work done in the experimental field.

The summary of the work presented herein is the result of a rather ambitious program undertaken by Convair to determine the flutter characteristics of a surface-piercing, supercavitating hydrofoil with a rudder or a spoiler type of control system as an integral part of the foil. It was the objective of this program to obtain parametric data on the effects on flutter stability of:

a. Control surface rotational resonant frequency.

b. Spoiler versus conventional trailing edge control surface.

c. Control surface chord.

d. Control surface angle.

e. Hydrofoil angle of attack.

In addition to these objectives, the effect of the depth of immersion was also investigated.

In general, the testing procedure followed a flight flutter testing procedure commonly used in the aircraft industry. That is, the flutter stability was determined by pulsing the test surface at increasing speeds and examining the resulting responses. The pulse was applied to the surface by cocking the control surface in the deflected position prior to the run and releasing it by a trip mechanism at the test velocity. This provided a section of the run with the surface in the deflected position, excitation to provide subcritical response and a section of the run in the trimmed position.
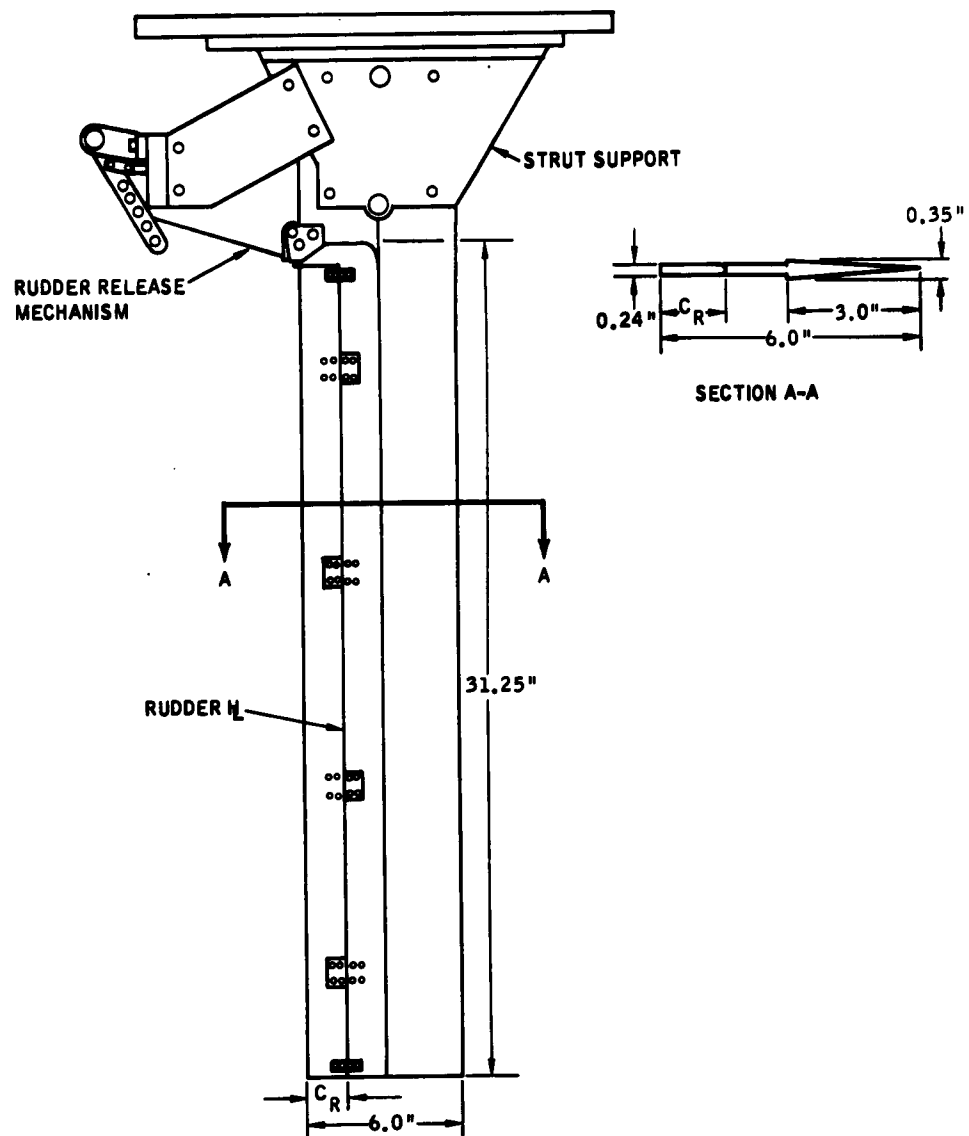
2 | FOIL DESIGN

The test foils are all-steel with a constant chord (including control surface) of six in. and a length of thirty in. The cross-section consists of a wedge-shaped forward semi-chord with a maximum depth of 0.35 in. and a constant depth trailing semichord of 0.24 in. Figures 1a, 1b and 2 show sketches of the foil configurations and a photo of the three rudder foils and two of the spoiler control surfaces. Foil R_2 received a permanent set during testing which may be seen in Figure 2. Table 1 is a summary of the foil mass characteristics.

2.1 FLEXURES

Each control surface was supported by flexures (Figure 3) which allowed the rotational frequency of the surfaces to be changed. These flexures were designed to obtain uncoupled rudder control surface natural frequencies of approximately 21, 55, and 90 cps and uncoupled spoiler natural frequencies of 30, 135, and 300 cps. The lowest frequency flexures proved too weak to withstand an extended test program largely due to a subcavitating flutter of the surface at velocities of 5 to 10 fps which had to be traversed on each run. This flutter mode was predominantly first foil bending and the flexures would not stand the large differential deflections encountered.

2.2 FOIL SPEED LIMITATIONS

Each foil was designed to an allowable limit stress of 190,000 psi in bending. The allowable limit speeds which resulted from this limitation are shown in Figures 4 through 7. Also shown in each figure is the divergence speed for each of the foils.

3

STRUT SUPPORT

RUDDER RELEASE
MECHANISM

0.35"

0.24" C_R 3.0"

6.0"

SECTION A-A

A   A

31.25"

RUDDER H_L

C_R

6.0"

Figure 1a.   Surface-Piercing Supercavitating Hydrofoil
Geometry — Rudder Model

4
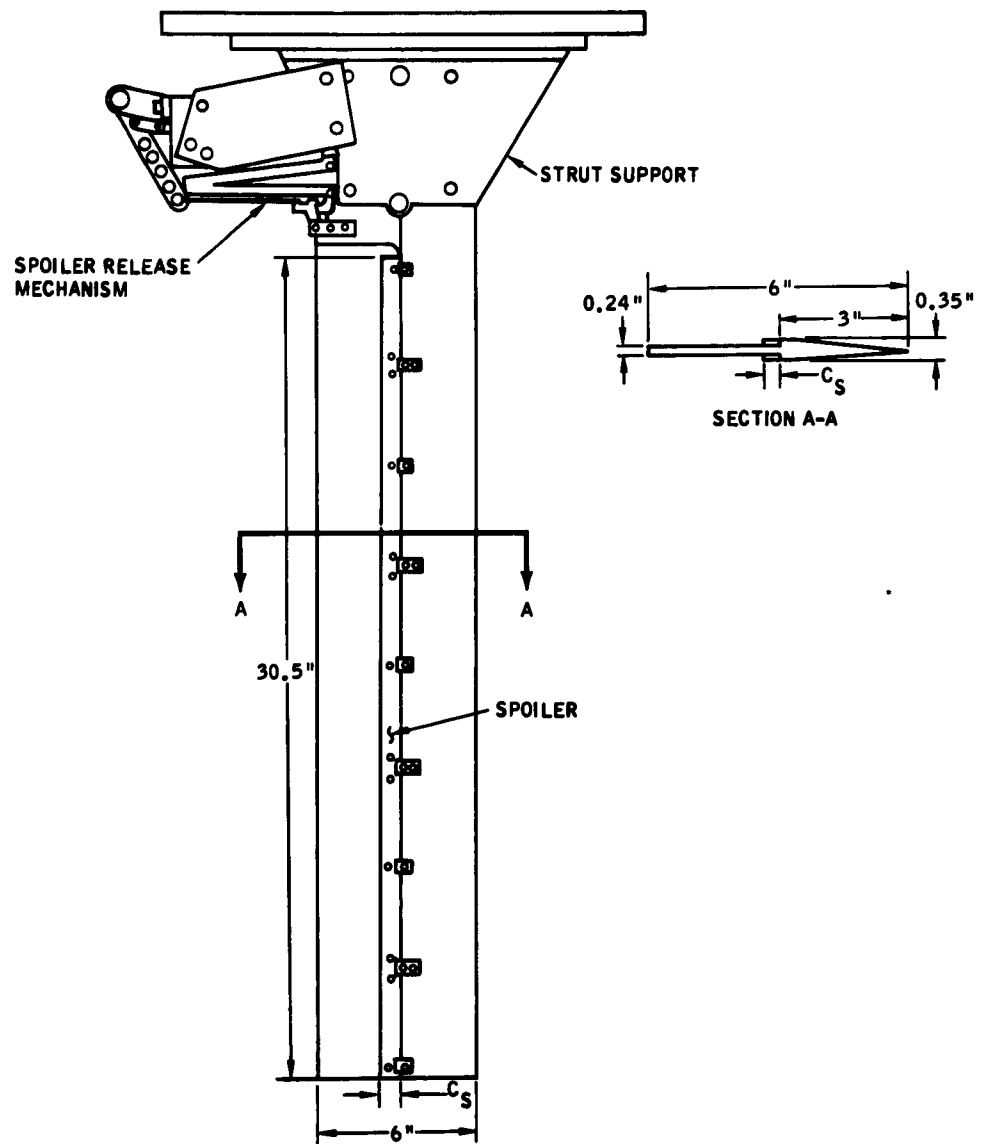
Figure 1b. Surface-Piercing Supercavitating Hydrofoil
Geometry — Spoiler Model

5

Table 1. Mass Characteristics of Foils

Configura-tion	Foil						Control Surface		
	Mass	I_x	I_p	J	x_α	r_α^2	Mass	I_y	x_α
	Slugs Per In.	In.^{4}	In.^{4}	In.^{4}			Slugs Per In.	In.^{4}	
R_1	.00903	.00509	1.5335	.02037	0	.1704	.00190	.06244	0.15
R_2	.00777	.00440	1.0619	.01761		.1180	.00316	.27690	0.25
R_3	.00651	.00371	.8495	.01485		.0944	.00443	.75054	0.35
S_1	.01093	.00612	2.9536	.02452		.3282	.00013	.00046	0.05
S_2	↓	↓	↓	↓	↓	↓	.00018	.00125	0.07
S_3	.01093	.00612	2.9536	.02452	0	.3282	.00026	.00363	0.10

Notes:

I_x = Cross section moment of inertia, axis along chord.

I_y = Cross section moment of inertia, axis normal to chord.

I_p = $I_x + I_y$

J = Polar moment of inertia as defined by Timoshenko in "Strength of Materials," Vol. II, denominator of equation 255, page 271.

x_α = Surface unbalance, non-dimensionalized by $x_\alpha = \dfrac{S_\alpha}{mb}$.

r_α = Dimensionless radius of gyration about elastic axis, in half-chord lengths; $r_\alpha^2 = I_\alpha / mb^2$.
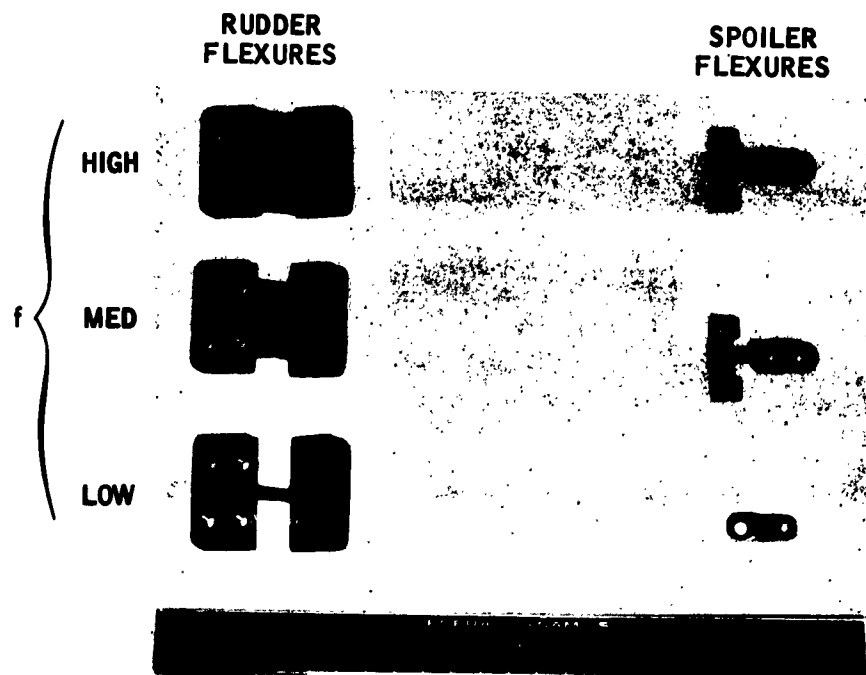
6

Figure 2.   Rudder Models

Figure 3.   Flexures

The carriage mounted on the hydrodynamic tank has nylon wheels with rubber inserts to damp excitation originating in the supporting rails. These wheels were designed originally for loads of 600 lb. This resulted in a limitation of foil velocity to keep these wheel loads to satisfactory levels and was controlled by calibrating the foils and reading the root bending moment on each run. This proved to be the limiting condition, especially at the higher angles of attack.

2.3 TRIP MECHANISM

The foil controls — rudder and spoilers — were held in a deflected position from the start of the run to the desired test point by a trip mechanism which held the rudder at the trailing edge at the root. This trip mechanism consisted of a sear that was released pneumatically by a solenoid signal at a fixed location along the track. The spoilers were held at four points along their spans to reduce the spoiler bending insofar as possible.
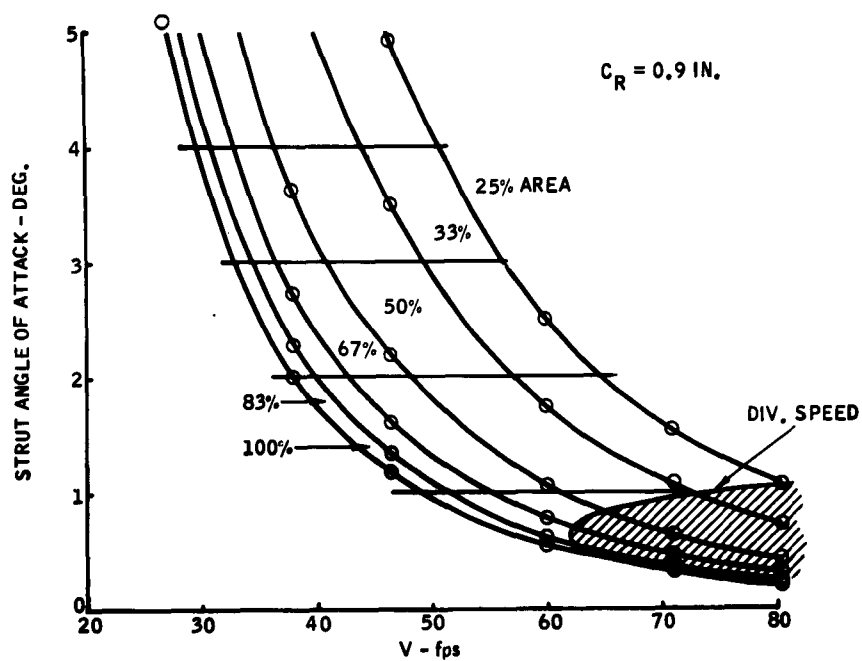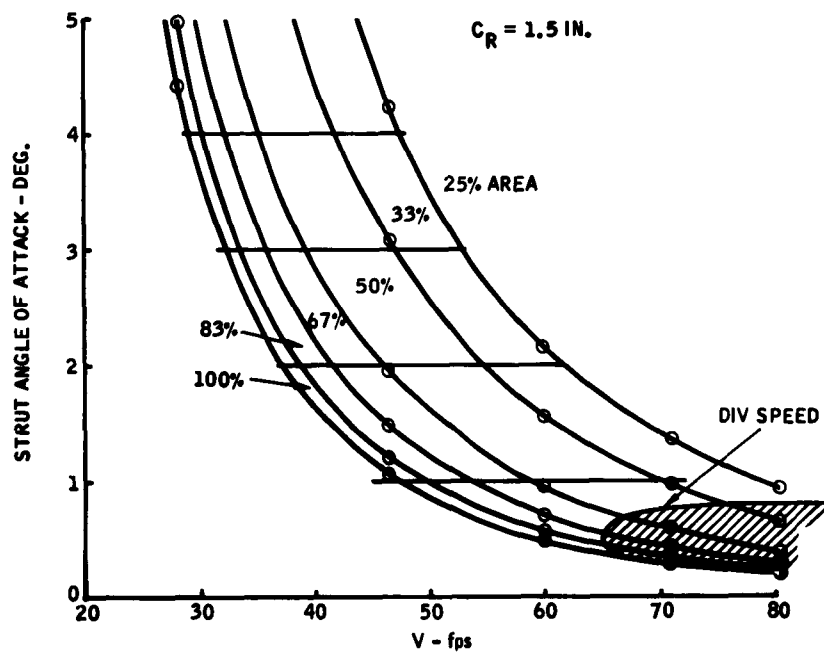
Figure 4.   Limit Speeds for Model R_1

Figure 5.   Limit Speeds for Model R_2
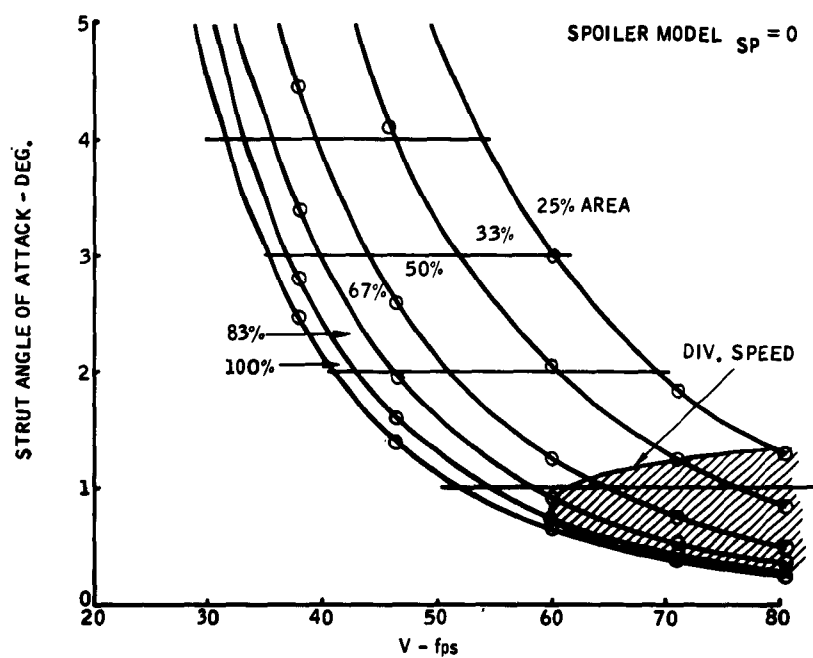
9

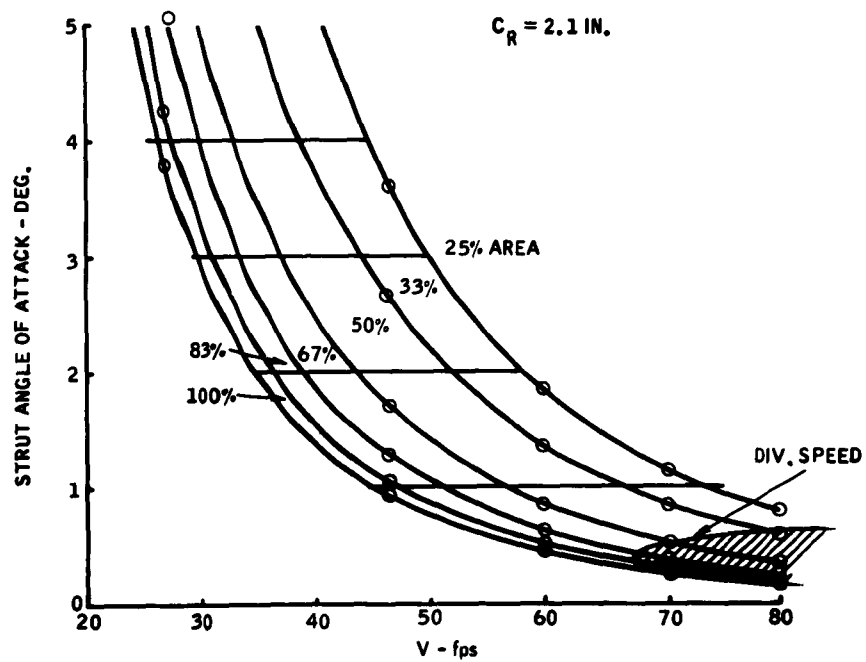Figure 6. Limit Speeds for Model R_3

Figure 7. Limit Speeds for Model S_n

3 | GROUND VIBRATION TESTS

A ground vibration test was accomplished on each foil surface to determine the natural frequencies and mode shapes. The mode shapes were determined for the surfaces vibrating in air and the natural frequencies were determined for the surface vibrating in air and in water.

3.1 TEST SETUP

The foils were mounted in the vertical position on a universal "Erector Set" type of test jig as shown in Figure 8. Excitation was provided by a small electromagnetic shaker sting-mounted at the end of the foil span. Two locations on the foil — leading edge and approximate mid-chord — were provided for the sting mounting.

The setup for the test in water used a 50-gallon drum in which a hole had been cut in the drum wall near the bottom. The excitation was provided by a small electromagnetic shaker with the sting through a rubber diaphragm in the tank hole. Figure 9 shows a view of this installation. The first three slosh modes of the drum are, theoretically, 1.4, 2.4 and 3.0 cps, which are well separated from the foil modes of interest. The important natural frequency of the system which was investigated consisted of the shaker mass-rubber diaphragm spring-mass system. By disconnecting the sting from the foil, installing an accelerometer on the sting near the diaphragm, and running a frequency sweep with the drum filled with water, a highly damped ($g \cong 0.15$) natural frequency of 28 cps was found. The amplitude of this response was small compared with the response of the foil, so that the foil natural frequency in this frequency range (second bending) was readily apparent and the response of the foil due to

11

Figure 8. Ground Vibration Test Setup — Air

Figure 9.   Ground Vibration Test Setup — Water

this shaker mass-diaphragm response could be seen as a small lobe near the base of the foil response curve.

The pumping action of the diaphragm would excite the foil bending modes with the sting connection to the foil disconnected. As might be expected, this pumping action would not excite the torsion modes of the foils.

3.2 DATA ACQUISITION

Three fixed accelerometer locations were used to develop frequency-response plots; a sample is shown in Figures 10 and 11. These plots were obtained by tracing on an X-Y plotter the rectified output of one of the three reference accelerometers as the frequency of excitation was slowly swept from 5 to 100 cps. The frequencies thus obtained were used as "target" frequencies, excitation was set up and varied until the maximum response was obtained, a decay record obtained of the response as the excitation was removed, and the mode shape measured by means of the "roving pickup technique. The same procedure was used in the test in the water except that the mode shapes were not measured.

3.3 RESULTS

The frequencies obtained from the ground vibration test are presented in Table 2. Table 3 presents the structural damping associated with each mode as measured from the decoys. This damping coefficient is:

$$g = 2\frac{c}{c_c} = \frac{1}{n\pi} \ln \frac{z_n}{z_o}$$

where:

$\dfrac{c}{c_c}$ = critical damping ratio

n = number of cycles over which damping is measured

z_n = amplitude of nth cycle

z_o = amplitude of initial cycle

l_n = natural logarithm
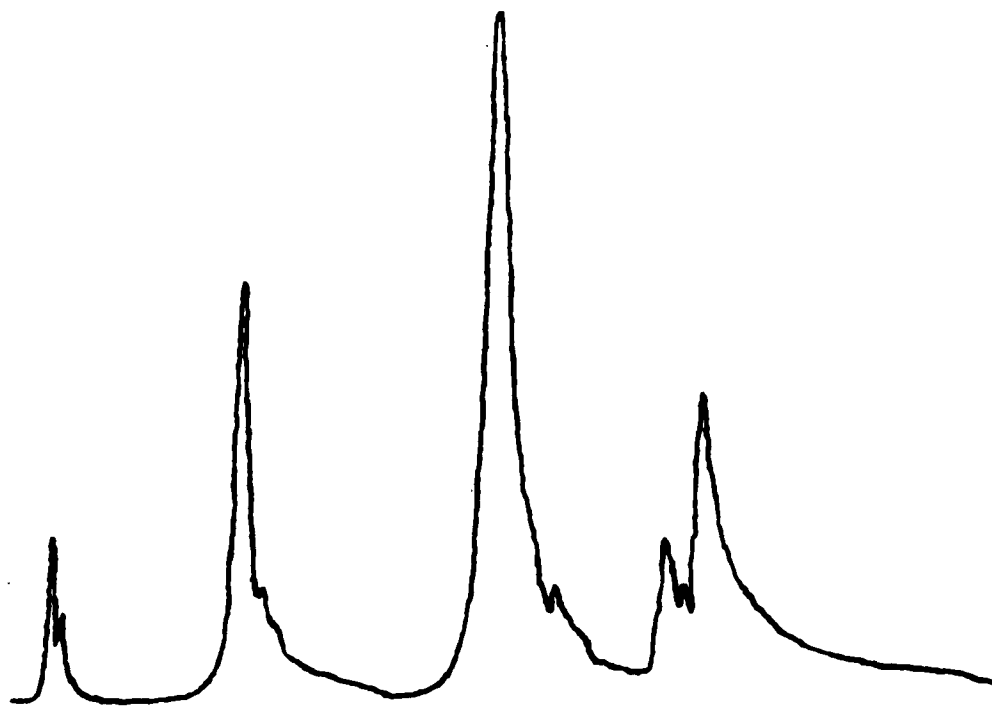
14

Figure 10. Sample X-Y Plot, Model R_1F_1 — Air

Figure 11. Sample X-Y Plot, Model R_1F_1 — Water

Table 2. Strut Resonant Frequencies

	R_1F_1	R_1F_2	R_1F_3	R_2F_1	R_2F_2	R_2F_3	R_3F_1	R_3F_2	R_3F_3	S_1F_1	S_3F_1
Air First Bend	9.45	9.9	9.3	9.1	9.2	9.2	8.9	8.8	8.8	9.7	9.8
Second Bend	43.9	43.3	43.7	41.8	41.0	4.13	39.6	37.5	31.1	45.5	46.0
First Torsion	77.8	73.2	77.2	67.6	58.8	60.0	60.4	51.6	47.1	85.3	85.5
Third Bend	-	-	109.6	113.2	113.0	114.0	110.0	110.0	105.9	116.5	118.0
Water First Bend	5.6	5.6	5.5	5.7	5.8	5.6	5.5	5.4	5.5	5.8	5.8
Second Bend	24.5	24.5	24.2	23.9	24.2	24.0	22.8	22.4	20.7	25.3	25.9
First Torsion	50.5	46.6	47.8	44.6	37.6	40.0	39.0	34.0	29.1	53.2	53.5
Third Bend	70.1	69.5	69.8	68.9	68.7	68.7	65.0	64.8	65.2	69.9	70.4
Second Torsion	-	98.6	-	85.3	87.0	90.5	-	94.0	82.8	-	-

Table 3. Strut Damping

	R_1F_1	R_1F_2	R_1F_3	R_2F_1	R_2F_2	R_2F_3	R_3F_1	R_3F_2	R_3F_3	S_1F_1	S_3F_1
Air First Bend	.006	.006	.005	.006	.004	.005	.006	.006	.009	.010	.004
Second Bend	.007	.013	.009	.004	.008	.009	.010	.008	.037	.006	.014
First Torsion	.017	.019	.017	.012	.021	.010	.011	.005	.018	.002	.002
Third Bend	-	-	.031	.009	.008	.012	.010	.016	.014	.009	.024
Water First Bend	.044	.044	.040	.047	.047	.049	.070	.049	.055	.033	.038
Second Bend	.019	.016	.016	.017	.017	.018	.020	.021	.032	.010	.020
First Torsion	.015	.020	.033	.010	.017	.021	.009	.011	.025	.006	.014
Third Bend	.020	.017	.014	.026	.027	.019	.013	.010	.015	.011	.007
Second Torsion	-	.028	-	-	.024	.030	-	.029	.024	-	-

16

The mode shapes for each natural frequency in air are shown in Figures 12 through 53. Only one set of flexures and two spoilers were used on the ground vibration test of the spoiler models because it became apparent that all spoiler models would yield identical mode shapes.

The ratio of the natural frequency in water to the natural frequency in air varied from 55 to 67 per cent with an average of 61 per cent. The second bending mode ratio of 58 per cent was the greatest change, while the torsion mode ratio of 64 per cent exhibited the least change in frequency.
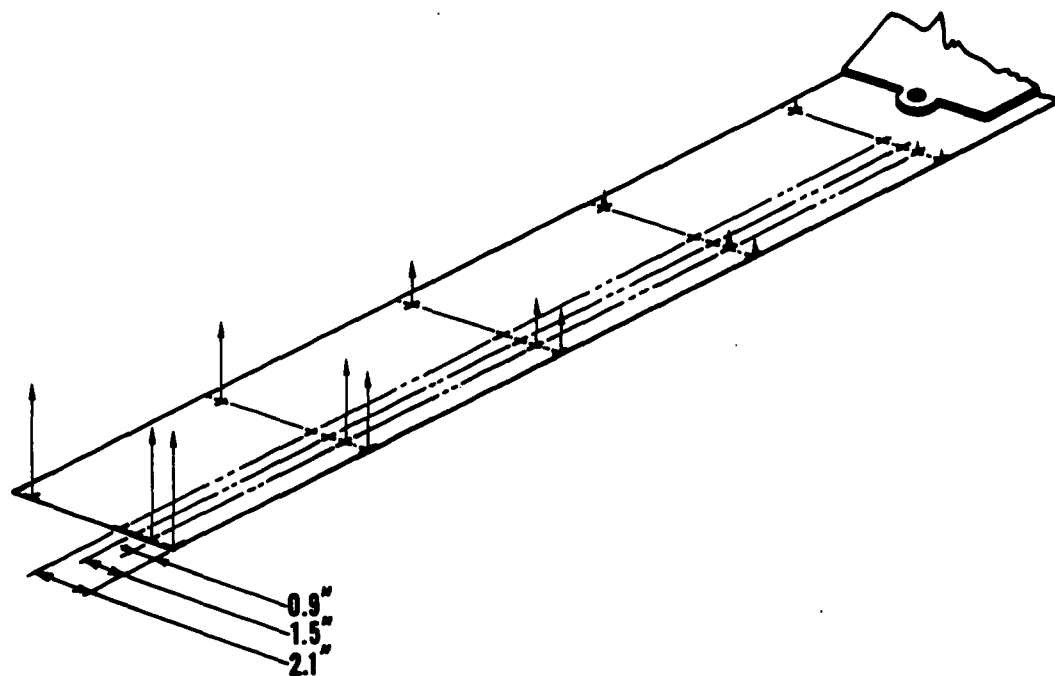
Figure 12.   Ground Vibration Test Mode Shape — Model R_1F_1, 9.45 cps, Damping Factor 0.0056
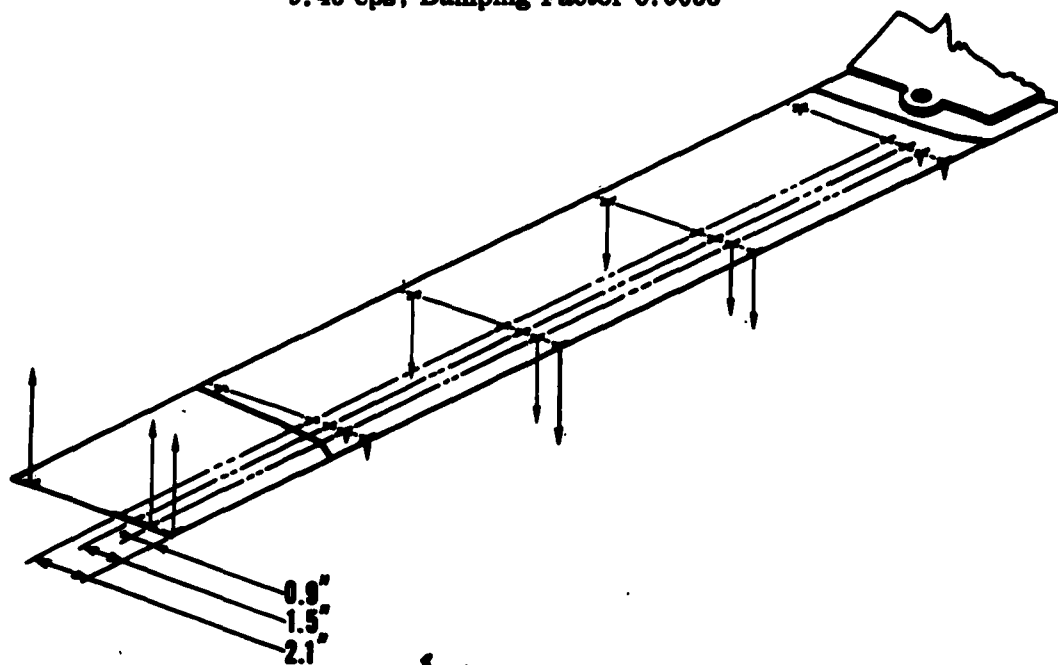
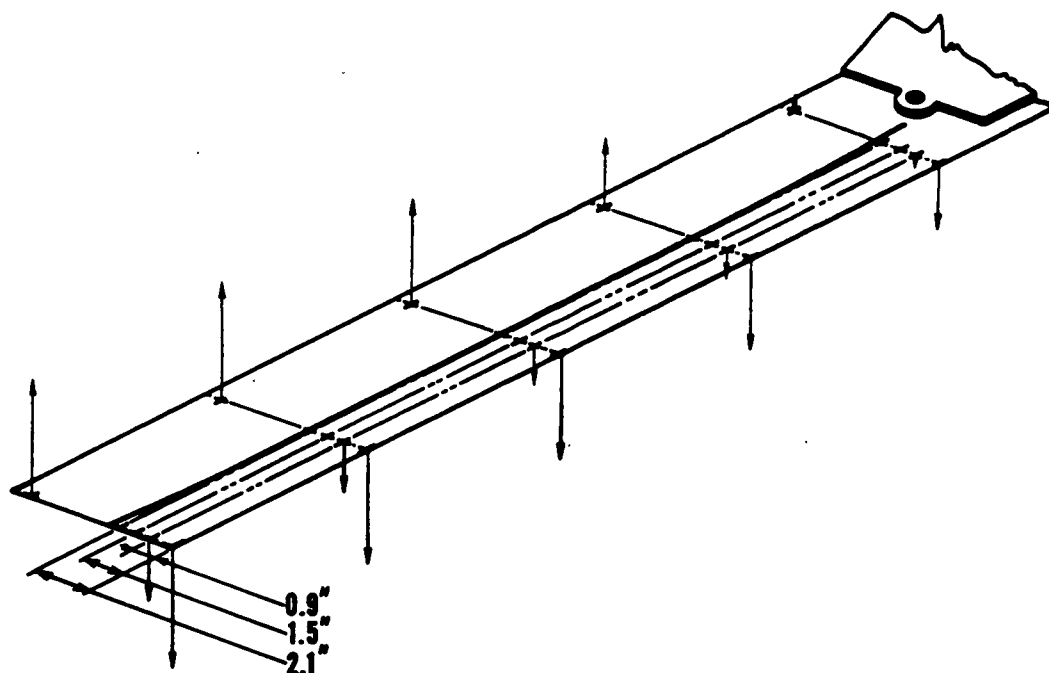Figure 13.   Ground Vibration Test Mode Shape — Model R_1F_1, 43.9 cps, Damping Factor 0.007

Figure 14.   Ground Vibration Test Mode Shape — Model R_1F_1,
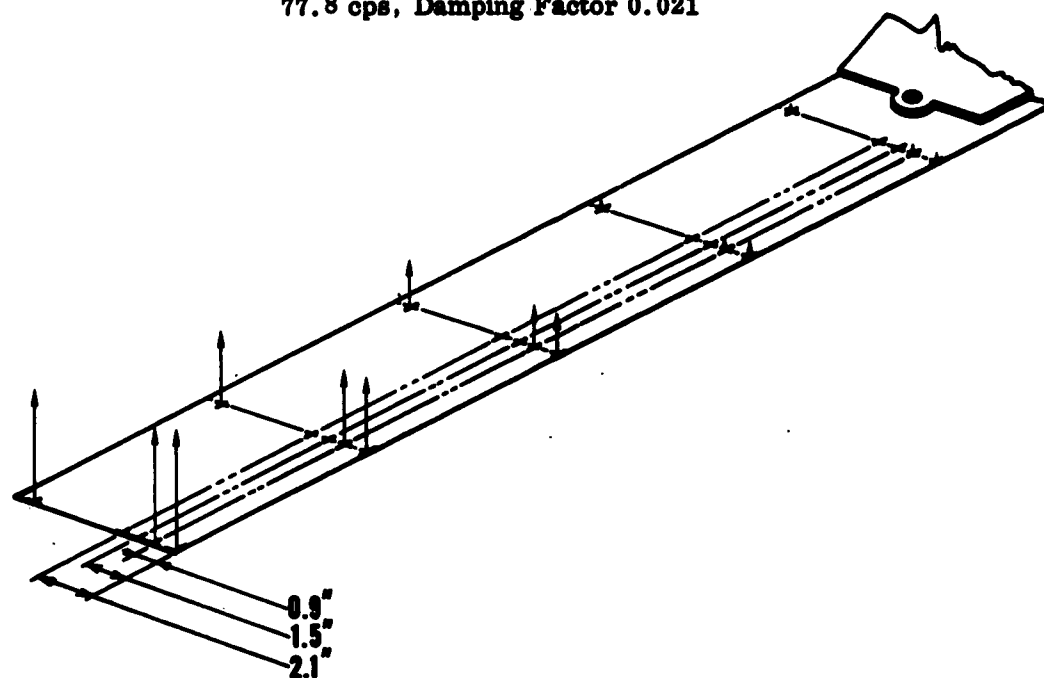77.8 cps, Damping Factor 0.021

Figure 15.   Ground Vibration Test Mode Shape — Model R_1F_2,
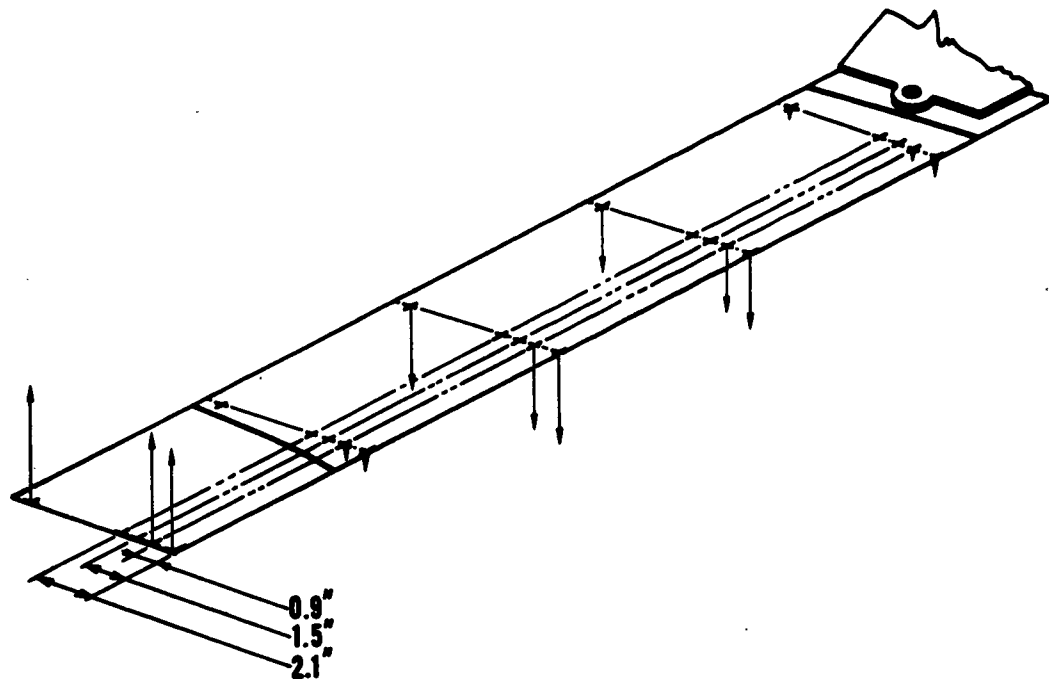9.9 cps, Damping Factor 0.006

19

Figure 16. Ground Vibration Test Mode Shape — Model R_1F_2, 43.3 cps, Damping Factor 0.013
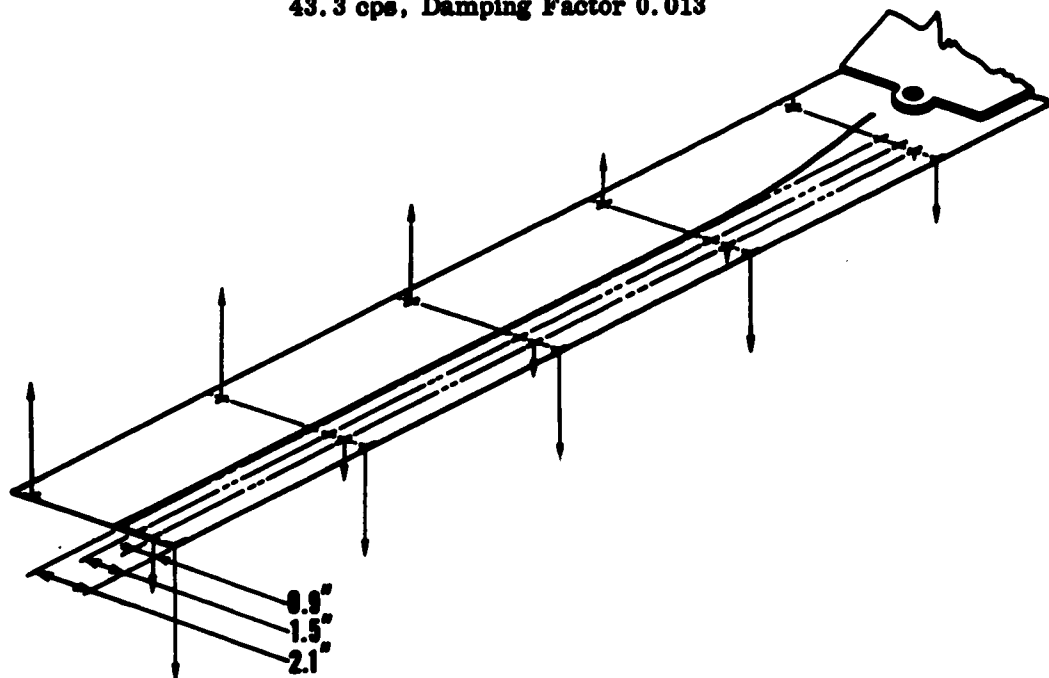

Figure 17. Ground Vibration Test Mode Shape — Model R_1F_2, 73.2 cps, Damping Factor 0.019

20

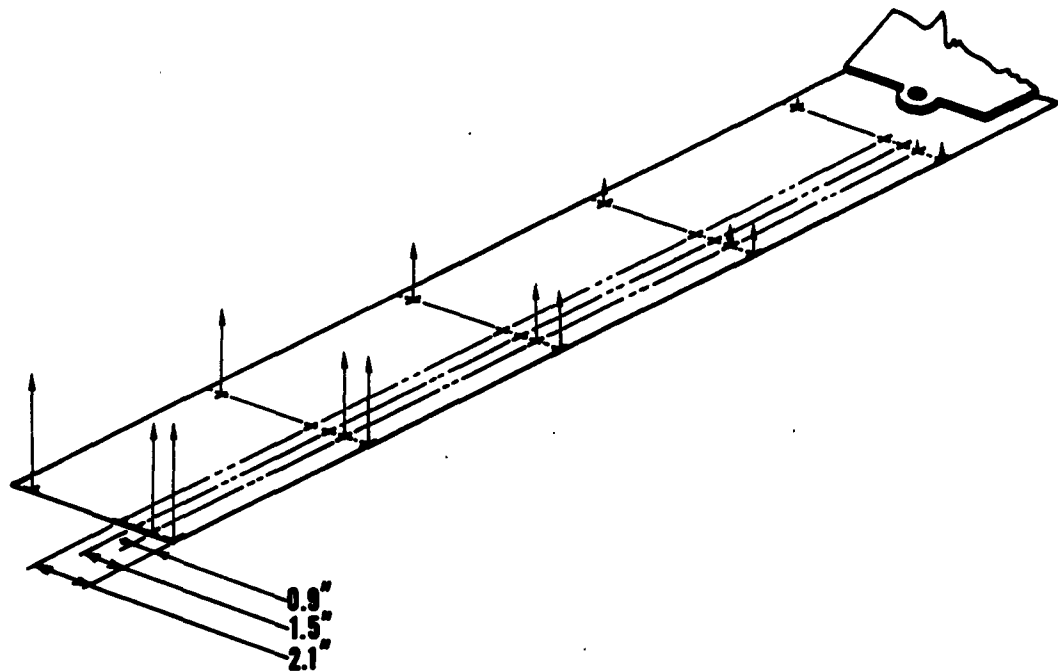Figure 18. Ground Vibration Test Mode Shape — Model R_1F_3, 9.3 cps, Damping Factor 0.005

Figure 19. Ground Vibration Test Mode Shape — Model R_1F_3, 43.7 cps, Damping Factor 0.009

0.9"
1.5"
2.1"

Figure 20. Ground Vibration Test Mode Shape — Model R_1F_3,
77.2 cps, Damping Factor 0.017

0.9"
1.5"
2.1"

Figure 21. Ground Vibration Test Mode Shape — Model R_1F_3,
109.6 cps, Damping Factor 0.031

Figure 22. Ground Vibration Test Mode Shape — Model R_2F_1, 9.1 cps, Damping Factor 0.0056
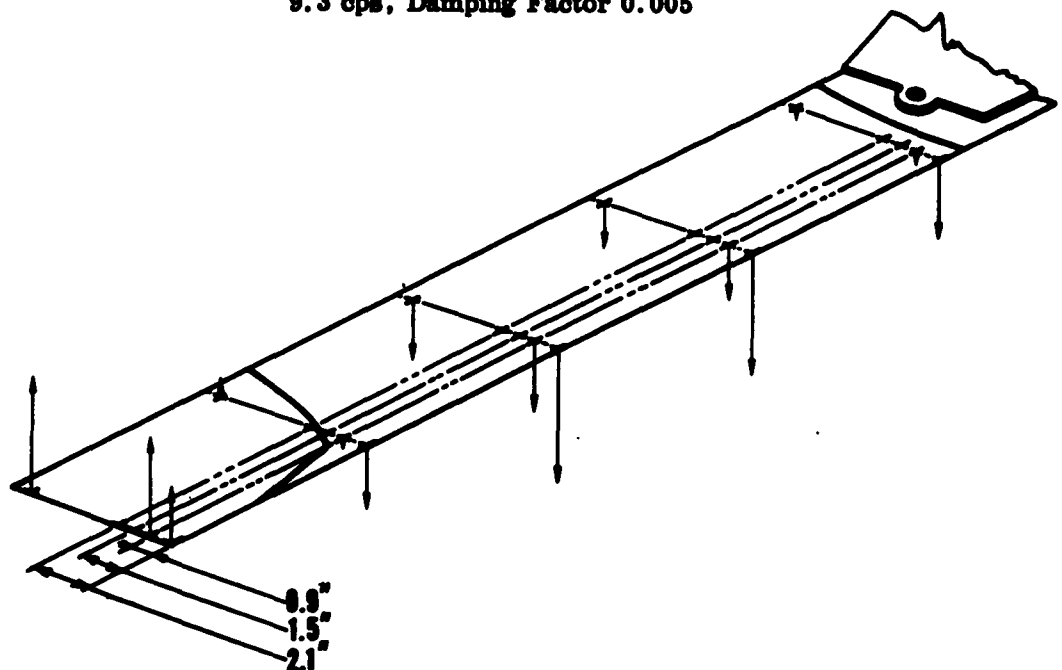

Figure 23. Ground Vibration Test Mode Shape — Model R_2F_1, 41.8 cps, Damping Factor 0.004

Figure 24. Ground Vibration Test Mode Shape — Model R_2F_1, 67.6 cps, Damping Factor 0.012

Figure 25. Ground Vibration Test Mode Shape — Model R_2F_1, 113.2 cps, Damping Factor 0.0094

24
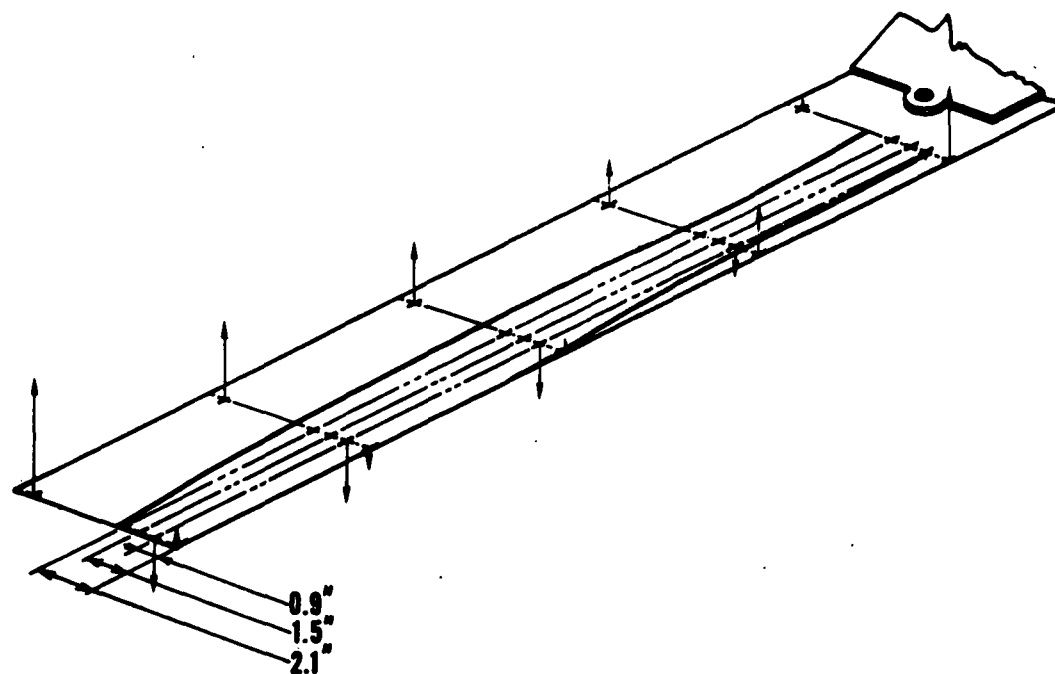
Figure 26. Ground Vibration Test Mode Shape — Model R_2F_2, 9.15 cps, Damping Factor 0.004

Figure 27. Ground Vibration Test Mode Shape — Model R_2F_2, 41.0 cps, Damping Factor 0.008

25

Figure 28. Ground Vibration Test Mode Shape — Model R_2F_2, 58.8 cps, Damping Factor 0.021

0.9"
1.5"
2.1"
2.1"

Figure 29. Ground Vibration Test Mode Shape — Model R_2F_2, 113.0 cps, Damping Factor 0.0083
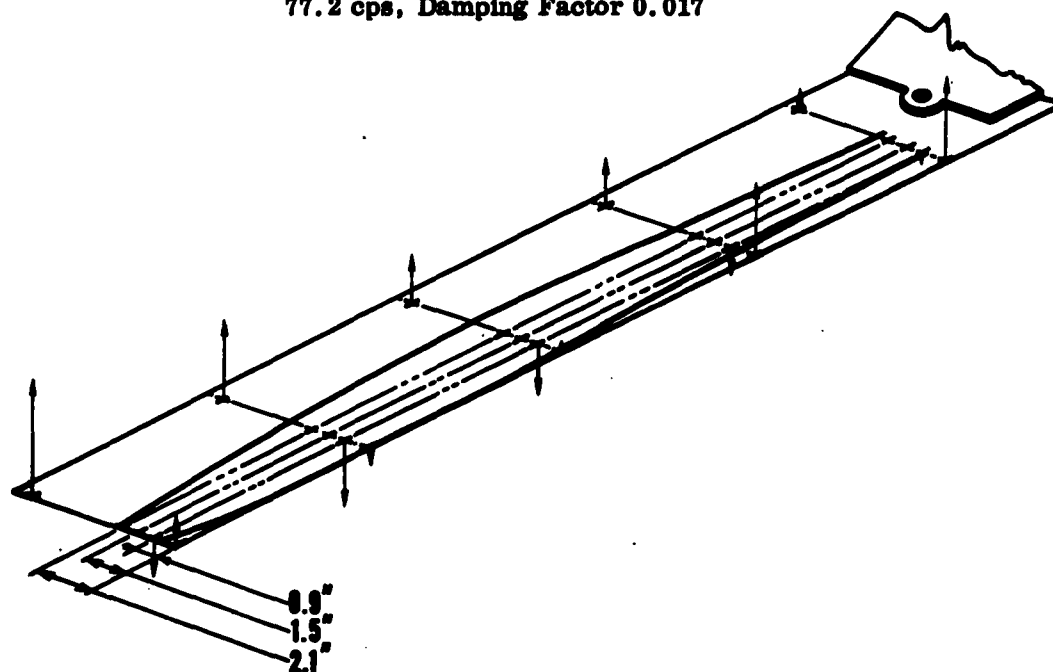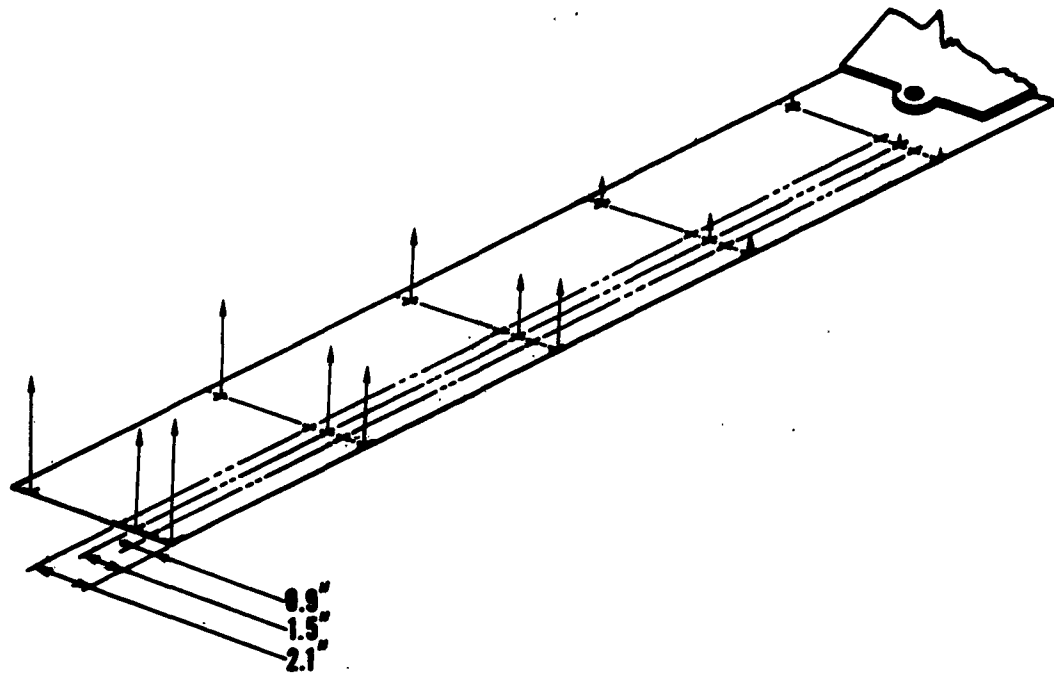
0.9"
1.5"
2.1"

26

Figure 30. Ground Vibration Test Mode Shape — Model R_2F_3,
9.15 cps, Damping Factor 0.005

Figure 31. Ground Vibration Test Mode Shape — Model R_2F_3,
41.3 cps, Damping Factor 0.009

27

Figure 32. Ground Vibration Test Mode Shape — Model R_2F_3, 60.0 cps, Damping Factor 0.010

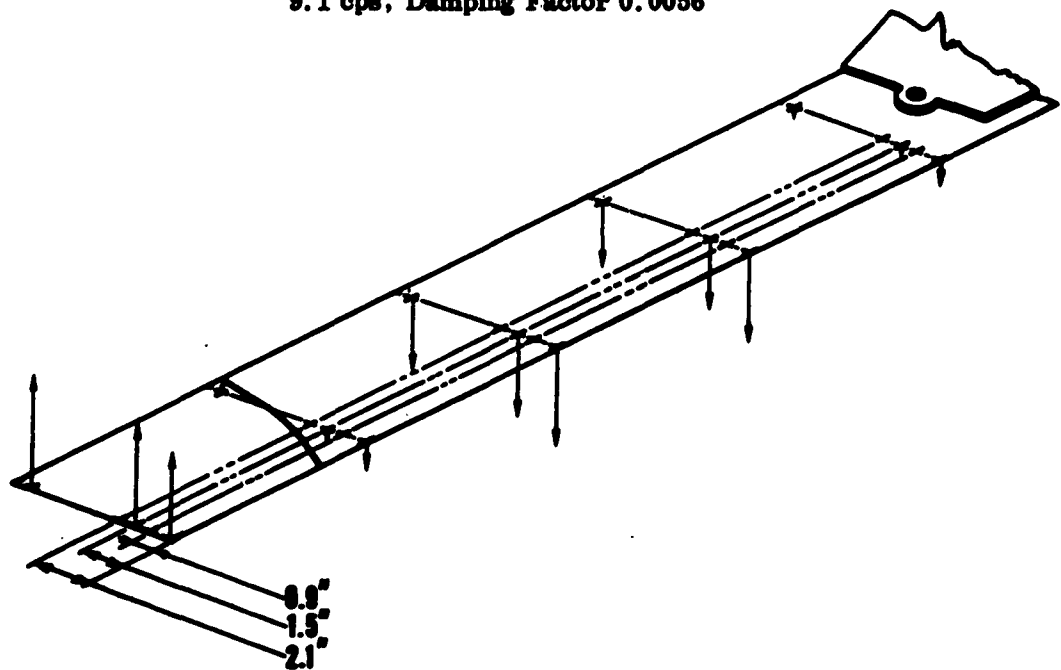

Figure 33. Ground Vibration Test Mode Shape — Model R_2F_3, 114 cps, Damping Factor 0.012

Figure 34. Ground Vibration Test Mode Shape — Model R_3F_1, 8.9 cps, Damping Factor 0.006

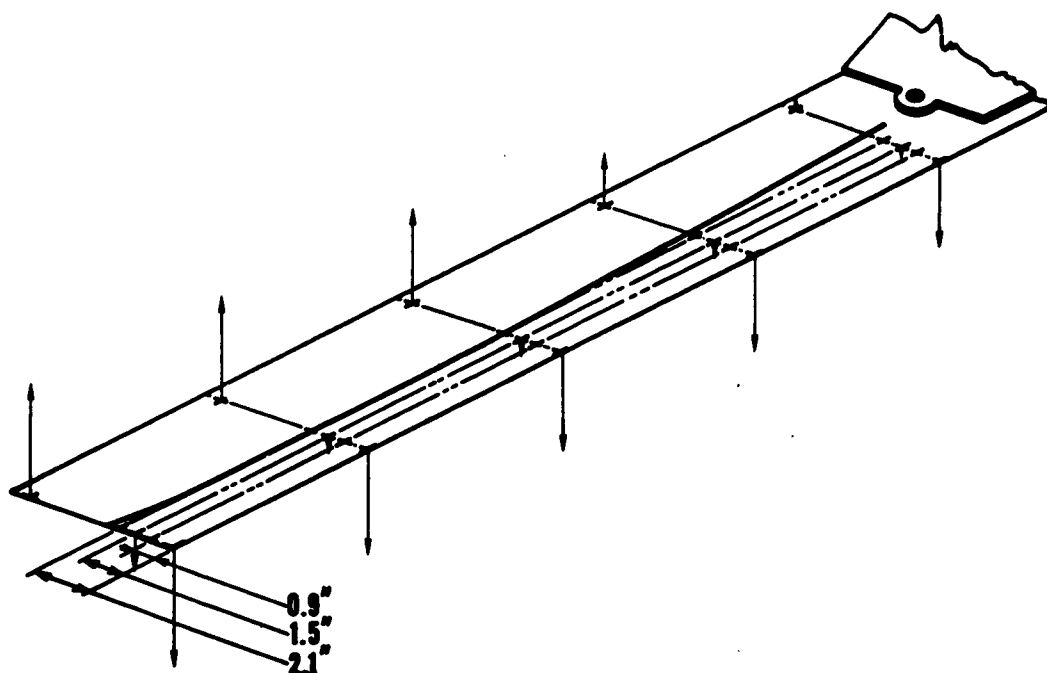Figure 35. Ground Vibration Test Mode Shape — Model R_3F_1 39.6 cps, Damping Factor 0.010

Figure 36. Ground Vibration Test Mode Shape — Model R_3F_1, 60.4 cps, Damping Factor 0.011
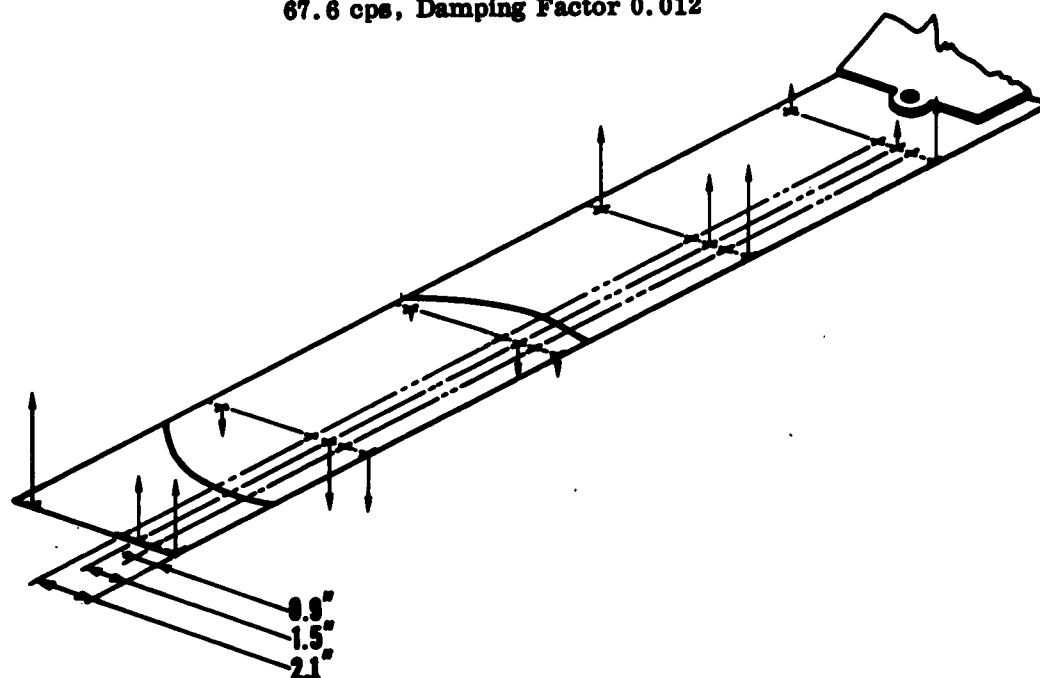

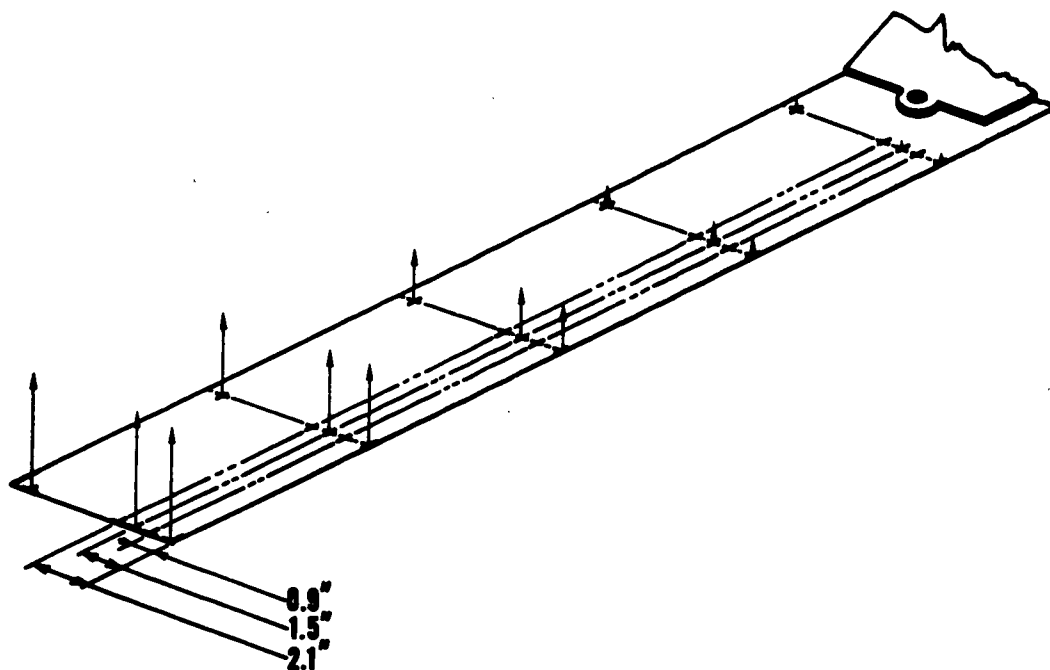Figure 37. Ground Vibration Test Mode Shape — Model R_3F_1, 110.0 cps, Damping Factor 0.010

Figure 38. Ground Vibration Test Mode Shape — Model R_3F_2, 8.8 cps, Damping Factor 0.006

Figure 39. Ground Vibration Test Mode Shape — Model R_3F_2, 37.5 cps, Damping Factor 0.008

31

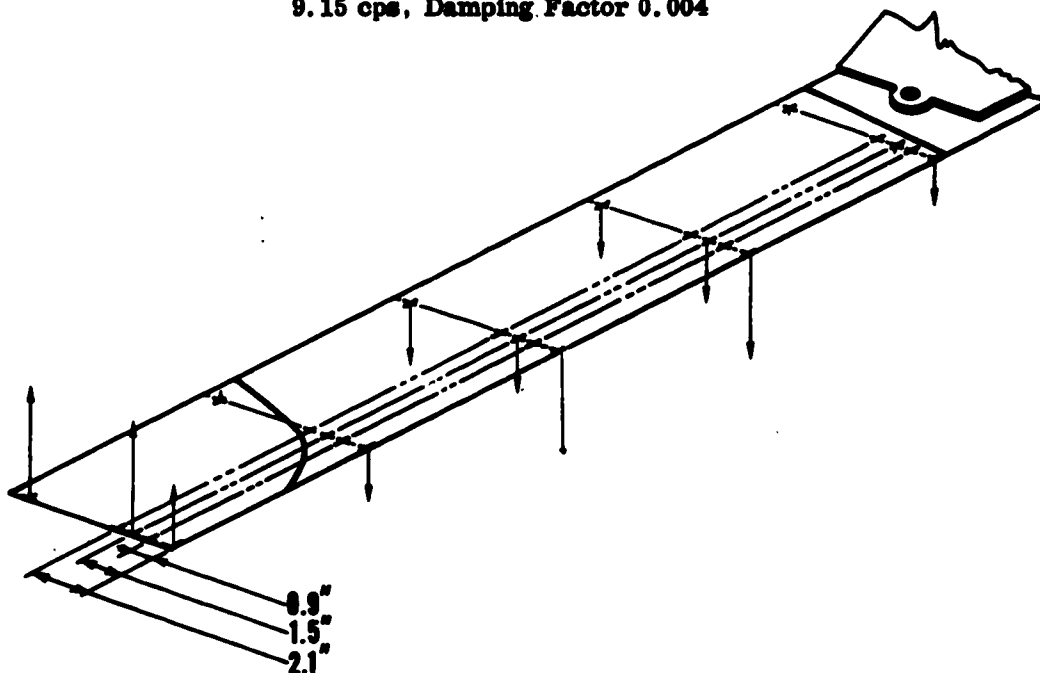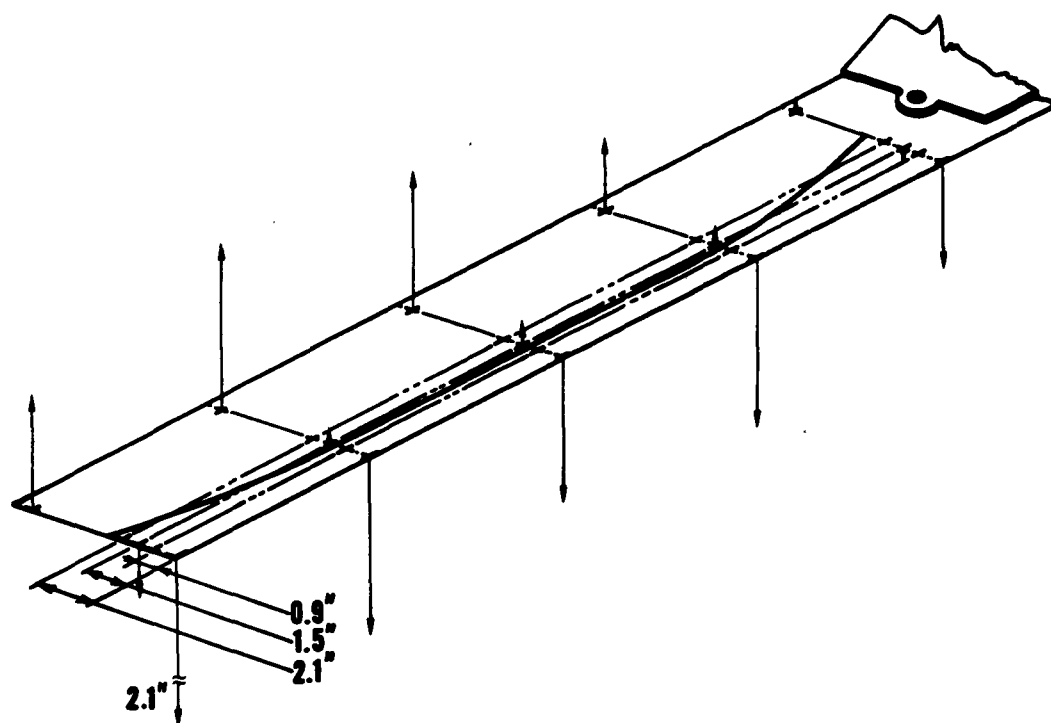Figure 40. Ground Vibration Test Mode Shape — Model R_3F_2, 51.6 cps, Damping Factor 0.005

Figure 41. Ground Vibration Test Mode Shape — Model R_3F_2, 110.0 cps, Damping Factor 0.016
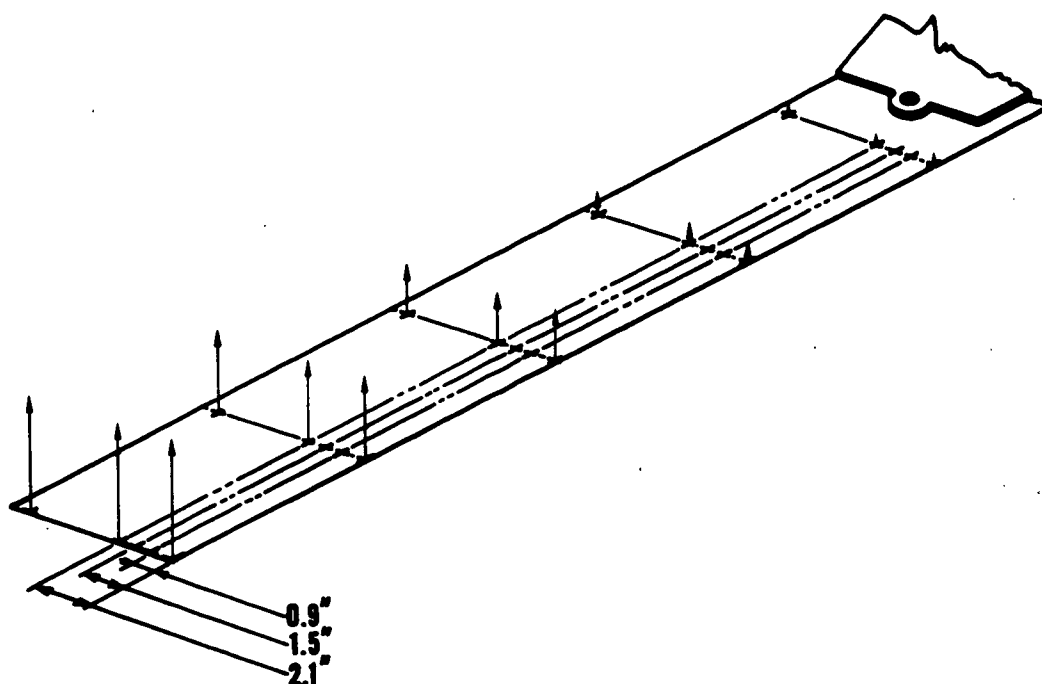
Figure 42. Ground Vibration Test Mode Shape — Model R_3F_3, 8.8 cps, Damping Factor 0.009
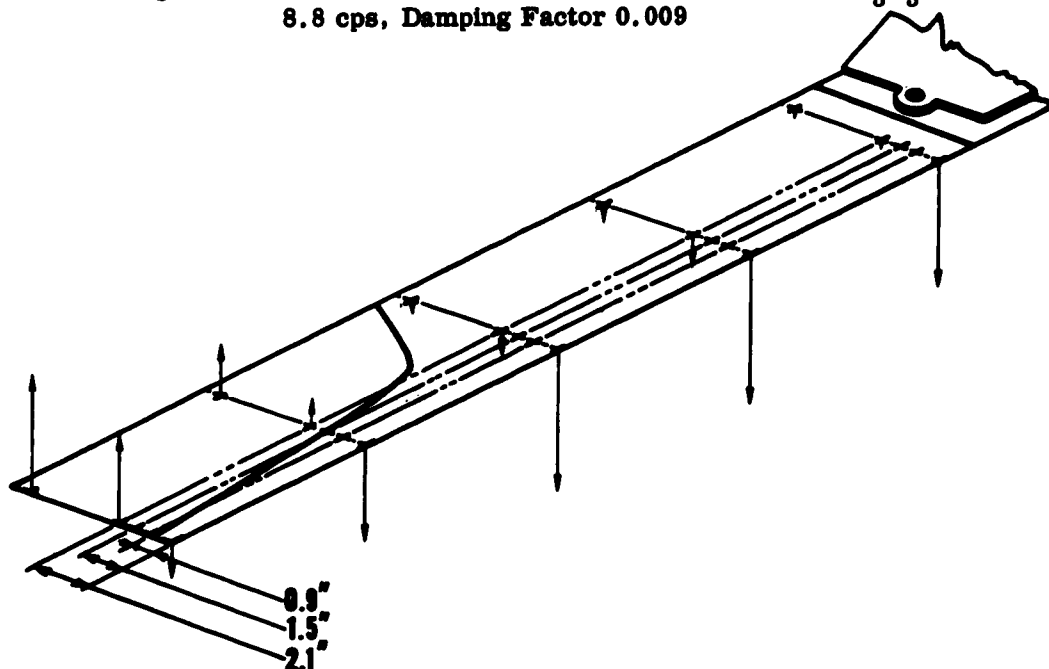
Figure 43. Ground Vibration Test Mode Shape — Model R_3F_3, 31.1 cps, Damping Factor 0.037

33
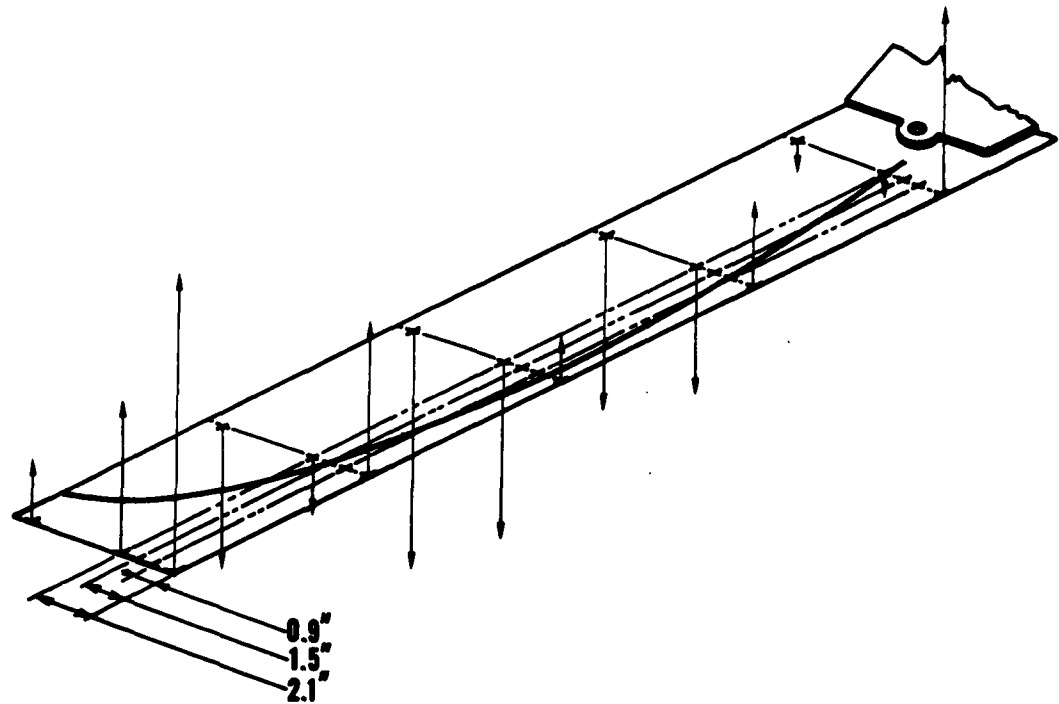
Figure 44. Ground Vibration Test Mode Shape — Model R_3F_3, 47.1 cps, Damping Factor 0.018
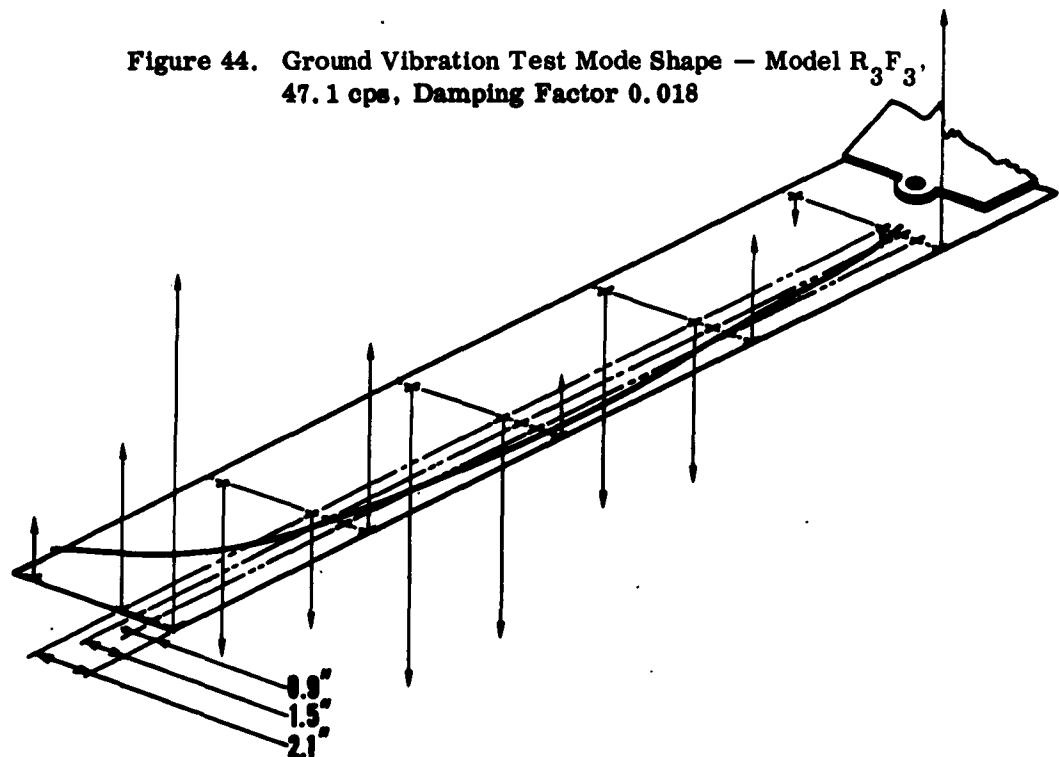
Figure 45. Ground Vibration Test Mode Shape — Model R_3F_3, 105.9 cps, Damping Factor 0.014

34
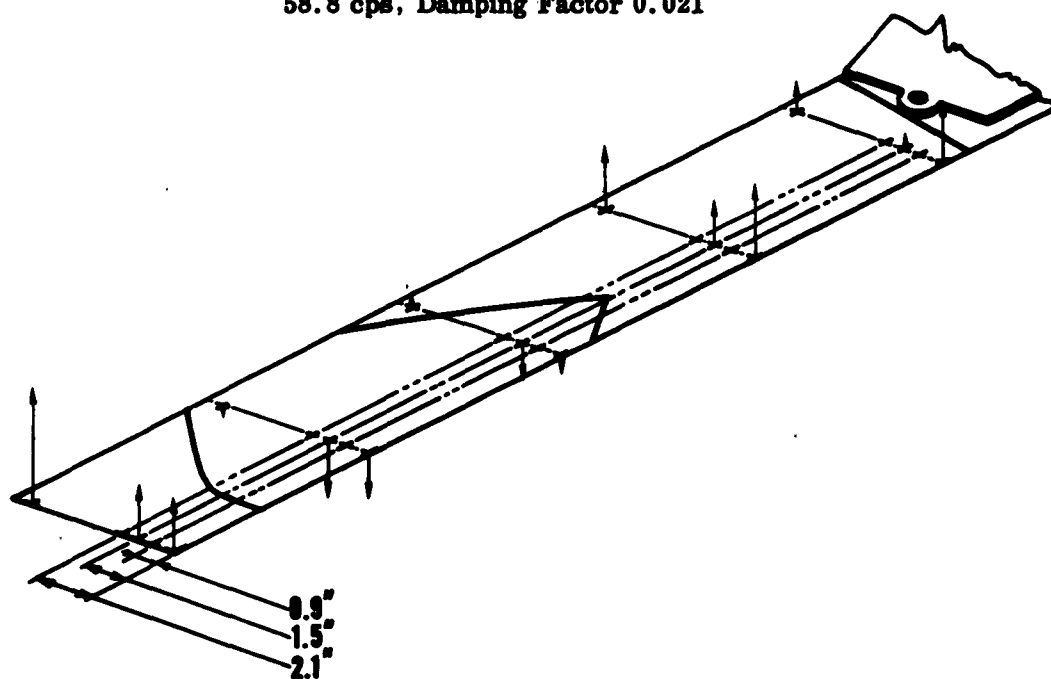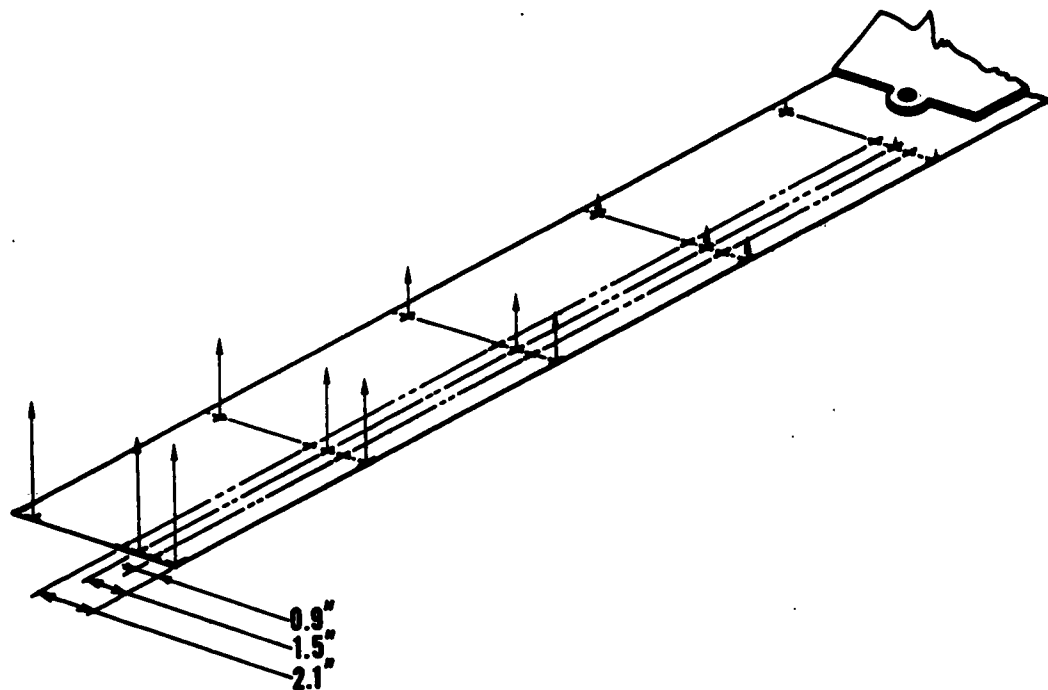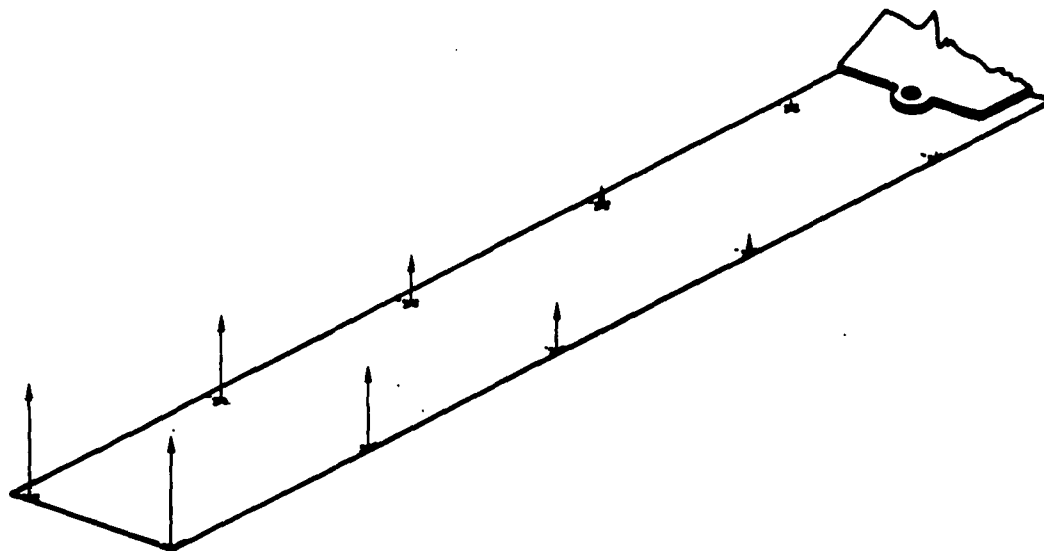
Figure 46. Ground Vibration Test Mode Shape — Model S_1F_1, 9.7 cps, Damping Factor 0.010
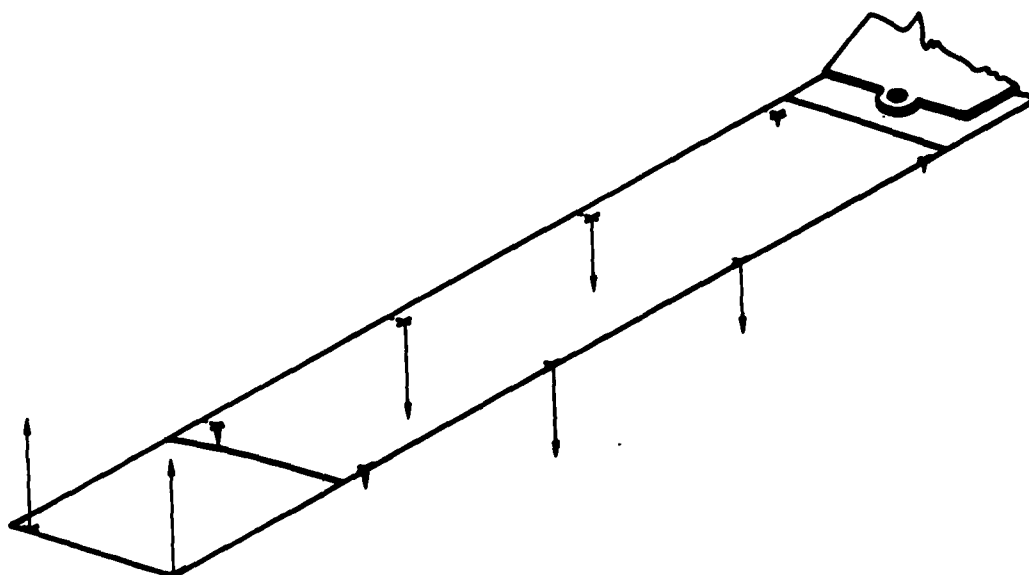
Figure 47. Ground Vibration Test Mode Shape — Model S_1F_1, 45.5 cps, Damping Factor 0.006
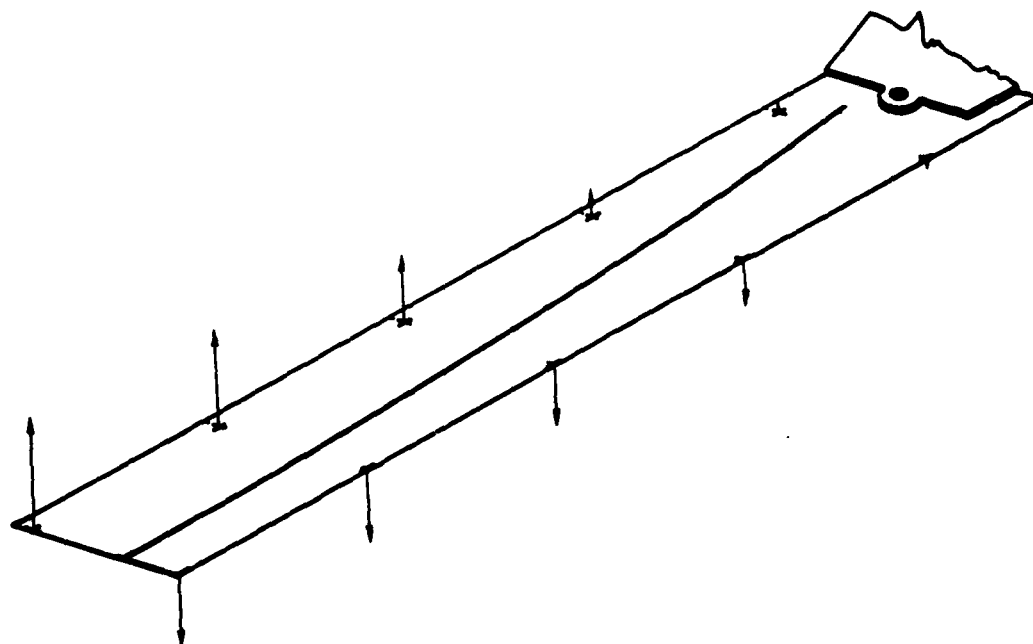
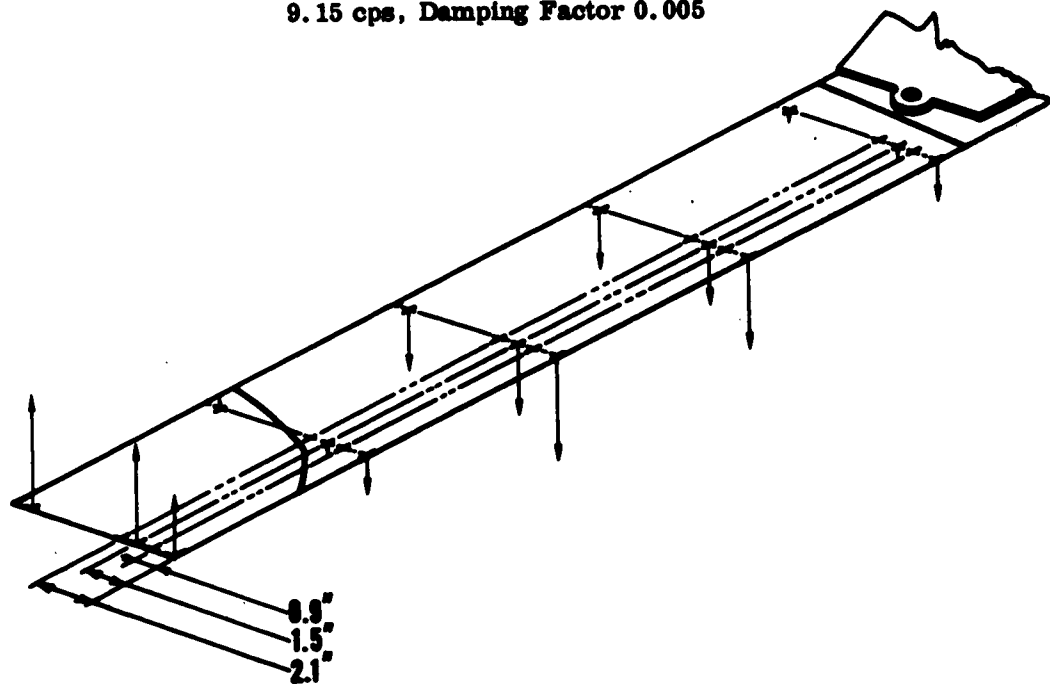Figure 48. Ground Vibration Test Mode Shape — Model S_1F_1, 85.3 cps, Damping Factor 0.002
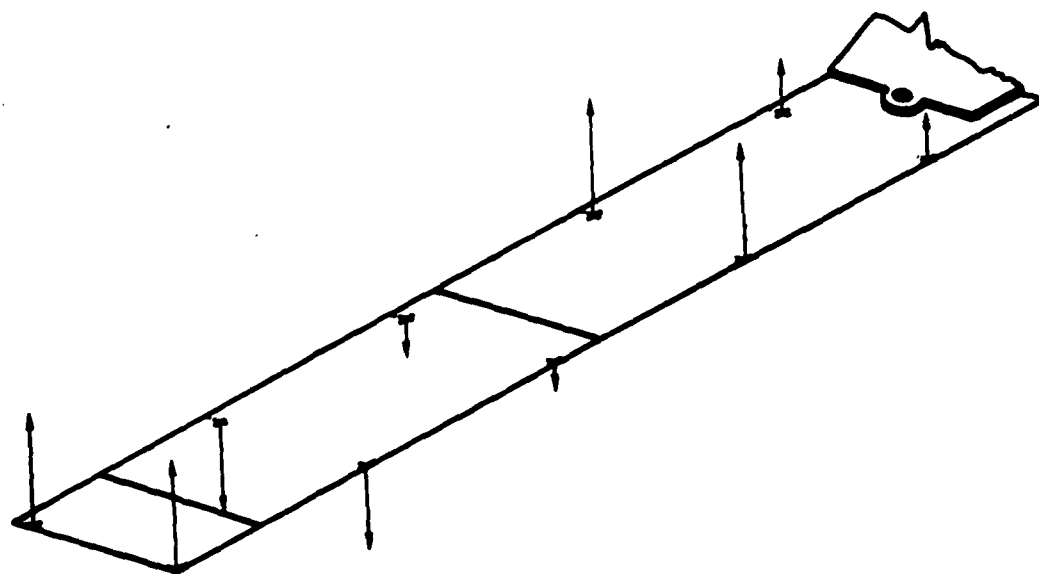
Figure 49. Ground Vibration Test Mode Shape — Model S_1F_1, 116.5 cps, Damping Factor 0.009
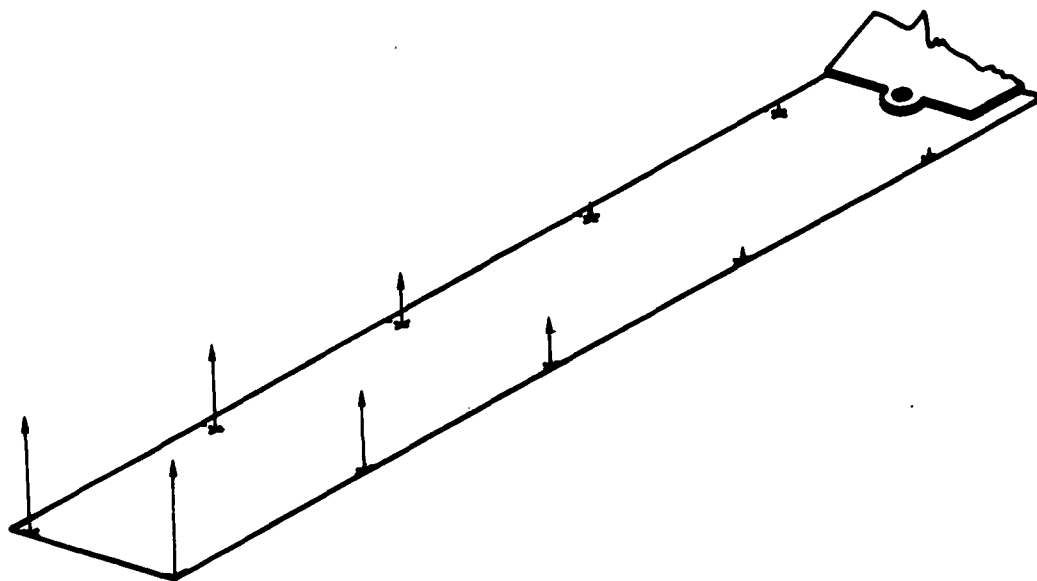
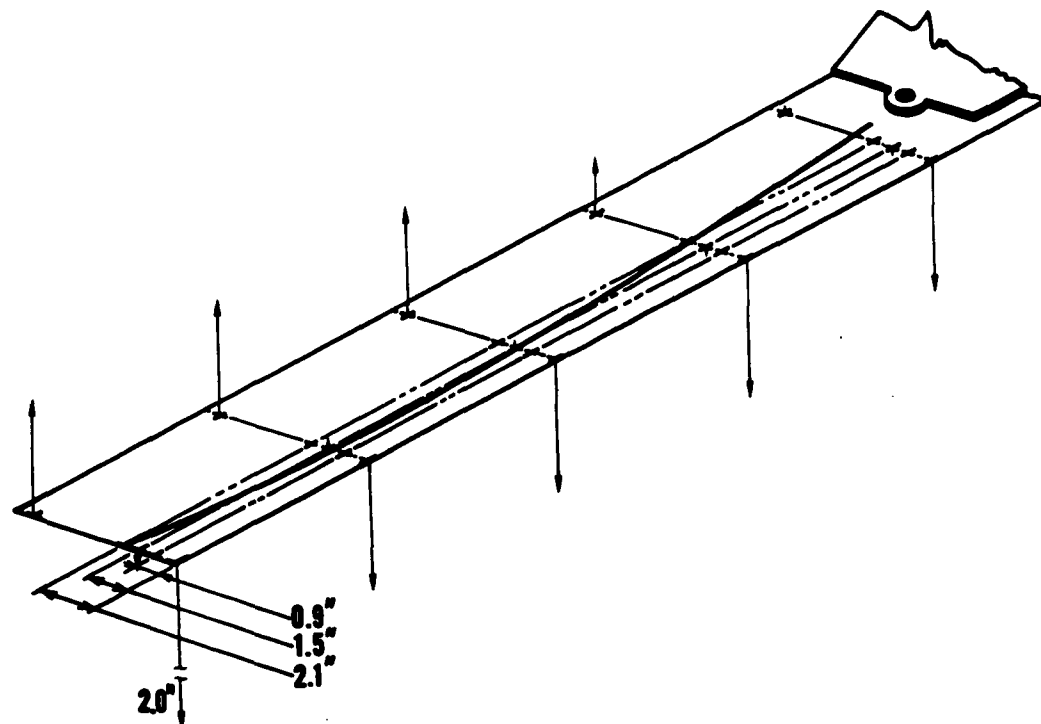Figure 50. Ground Vibration Test Mode Shape — Model S_3F_1, 9.8 cps, Damping Factor 0.004
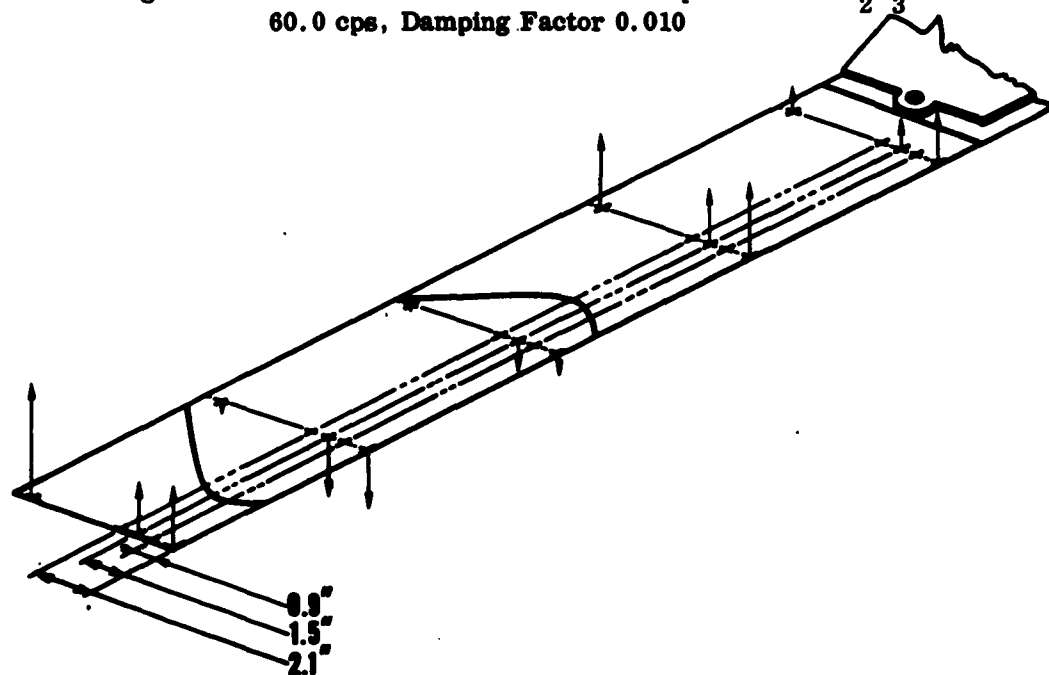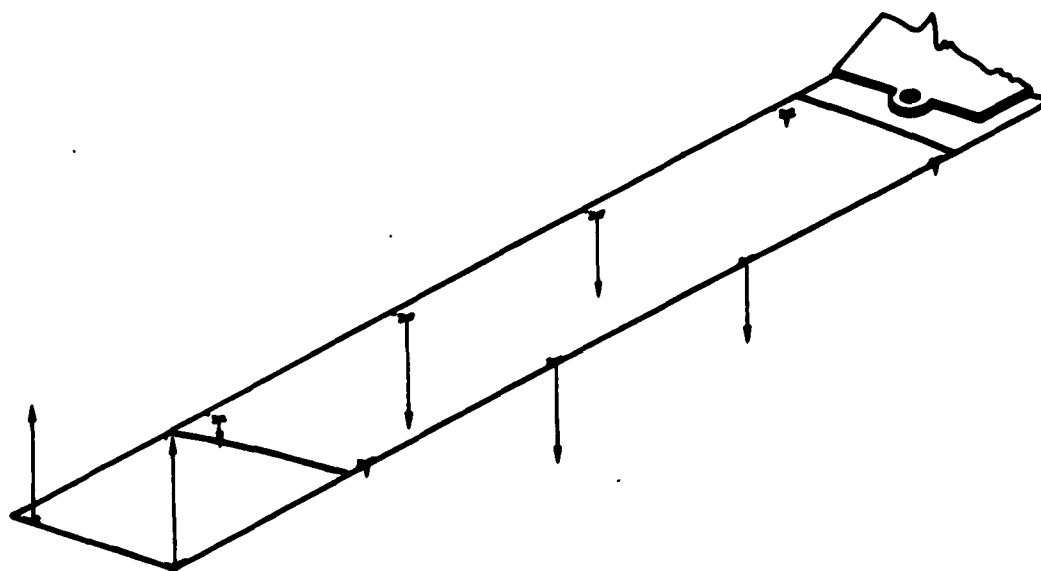

Figure 51. Ground Vibration Test Mode Shape — Model S_3F_1, 46.0 cps, Damping Factor 0.014
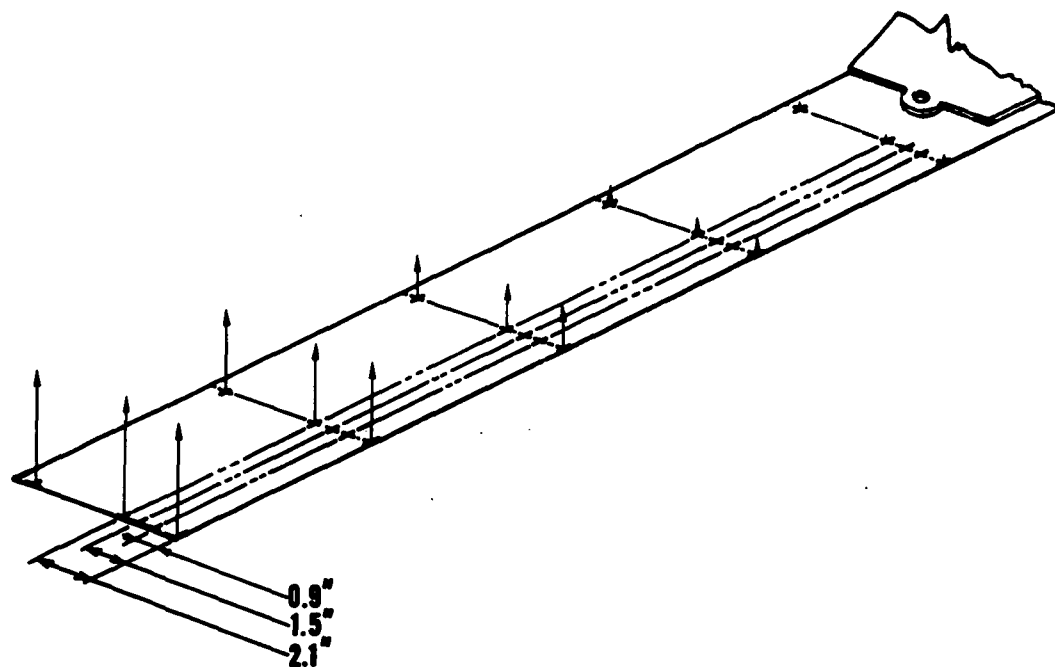
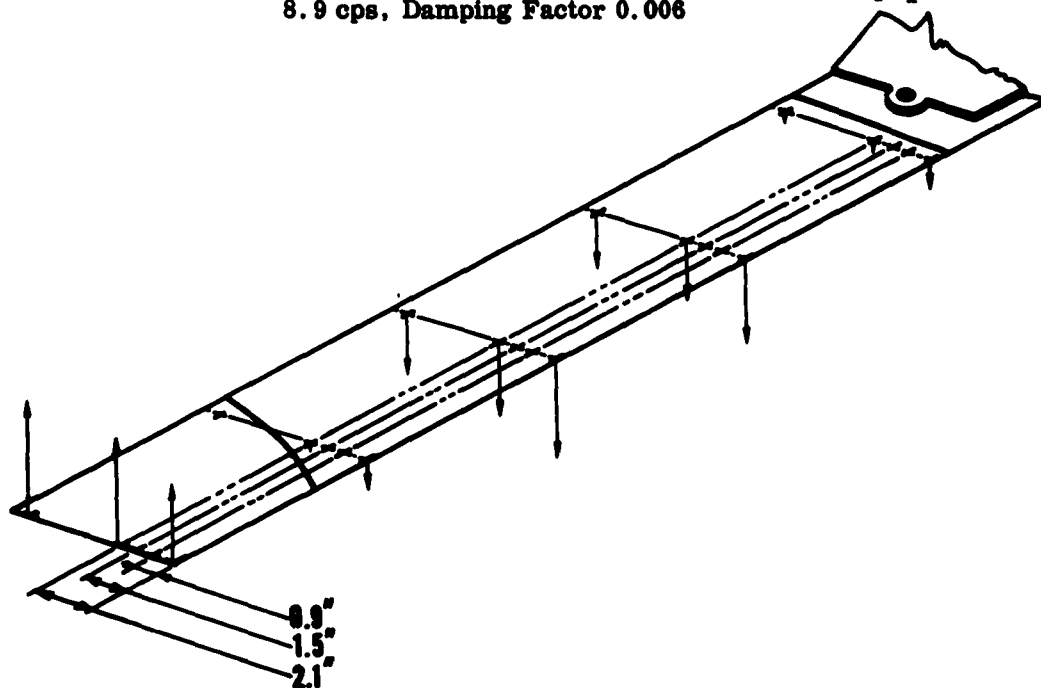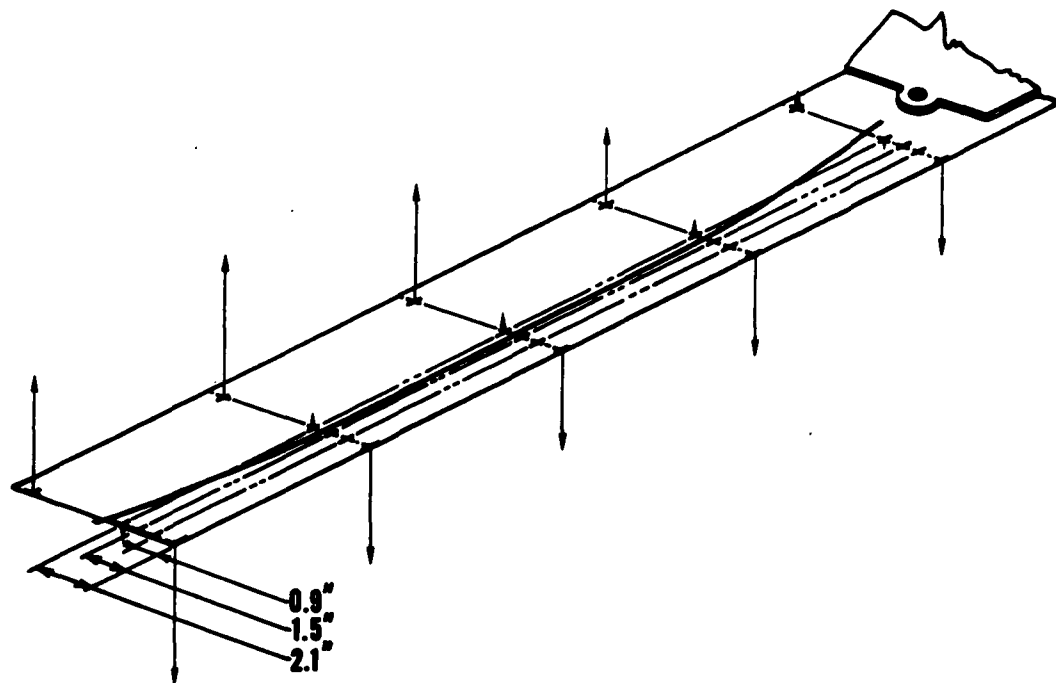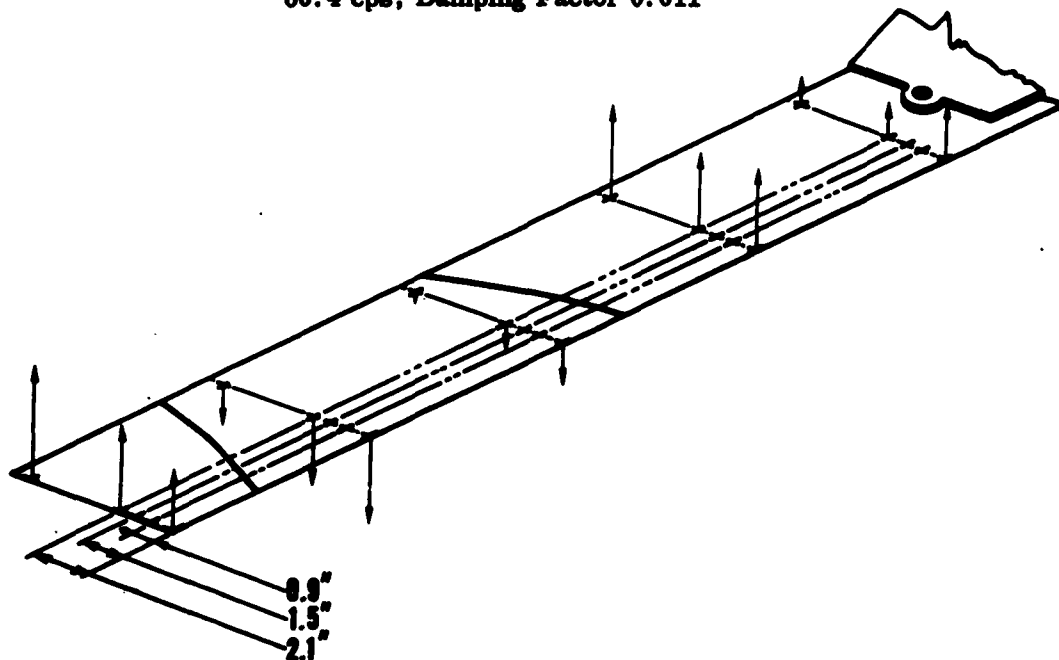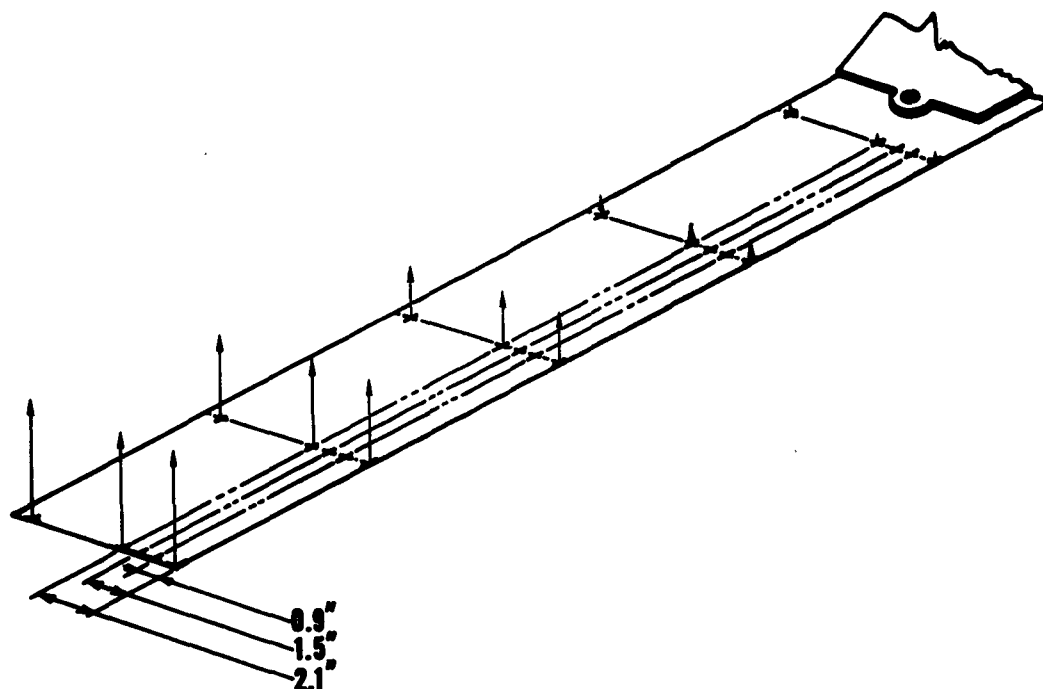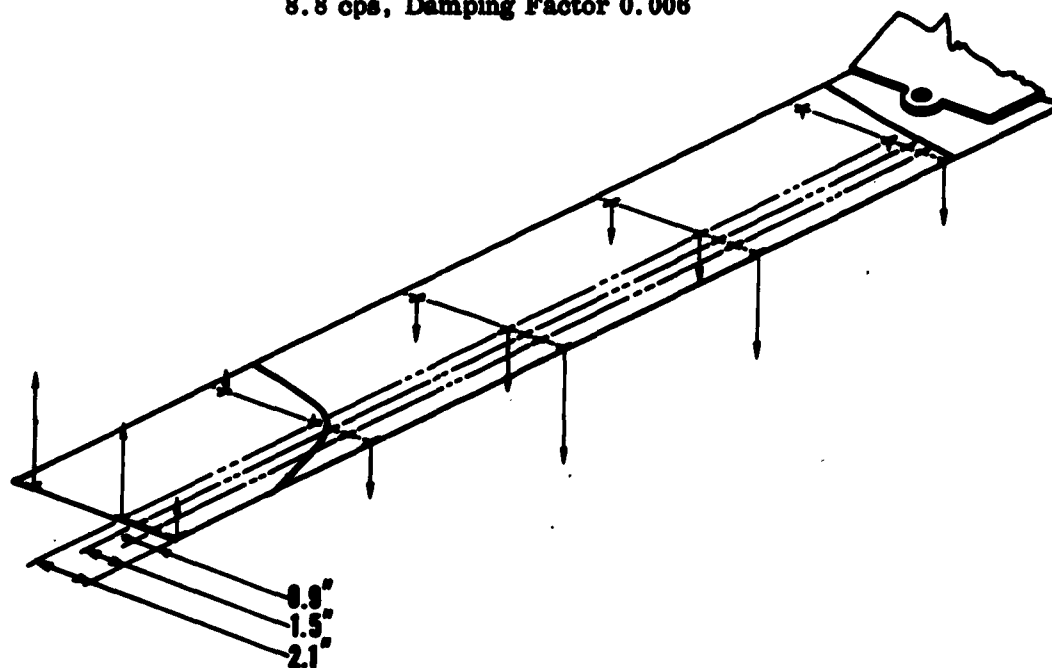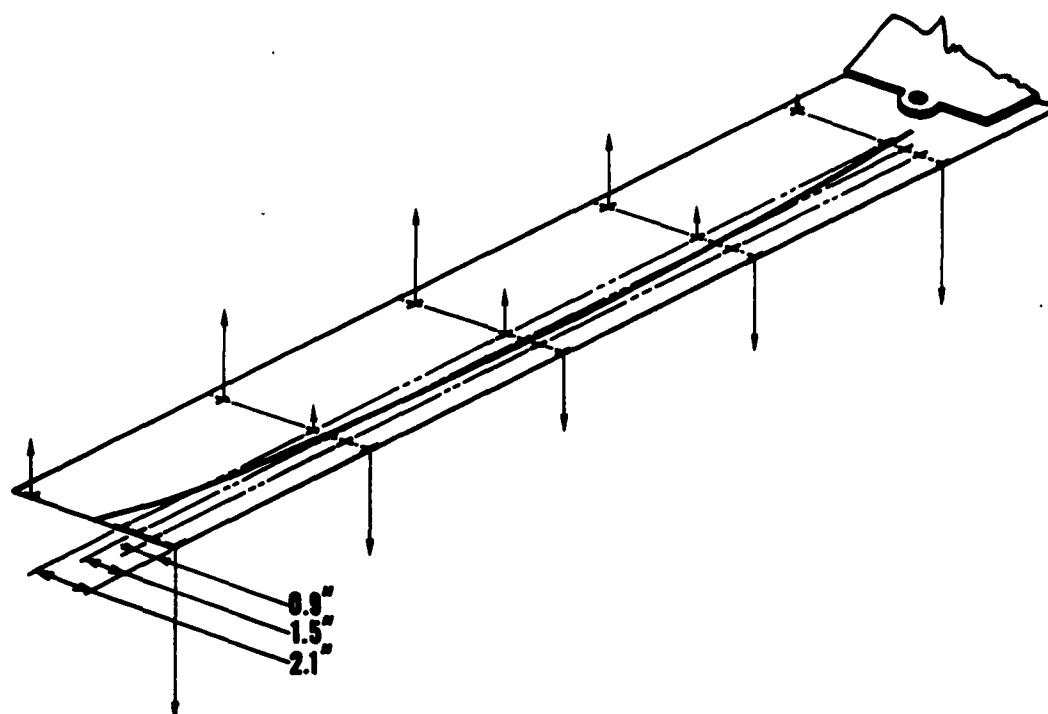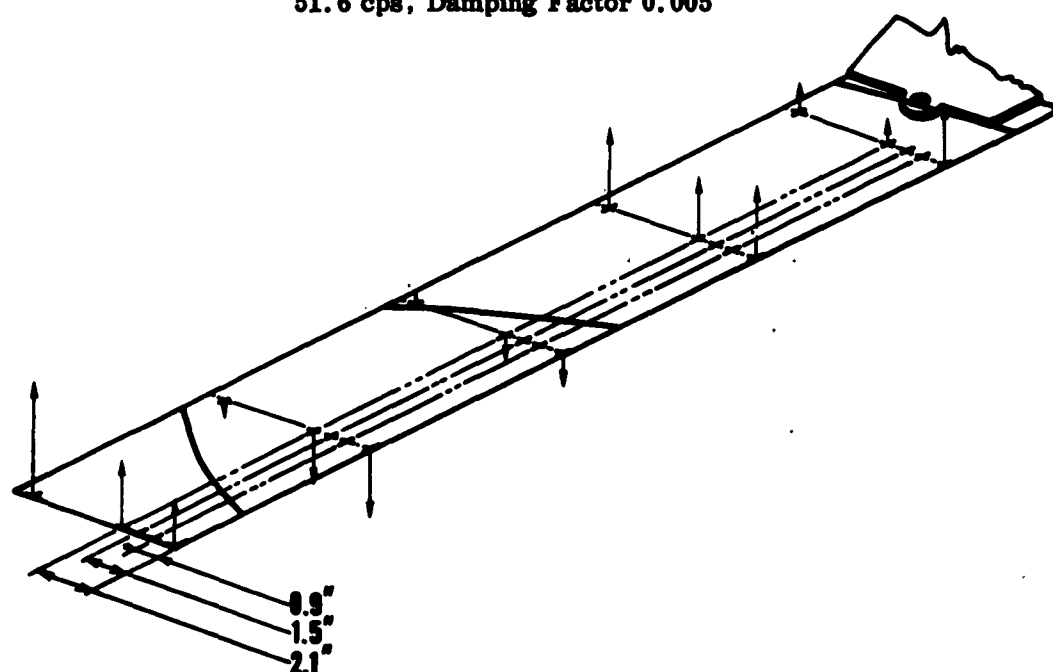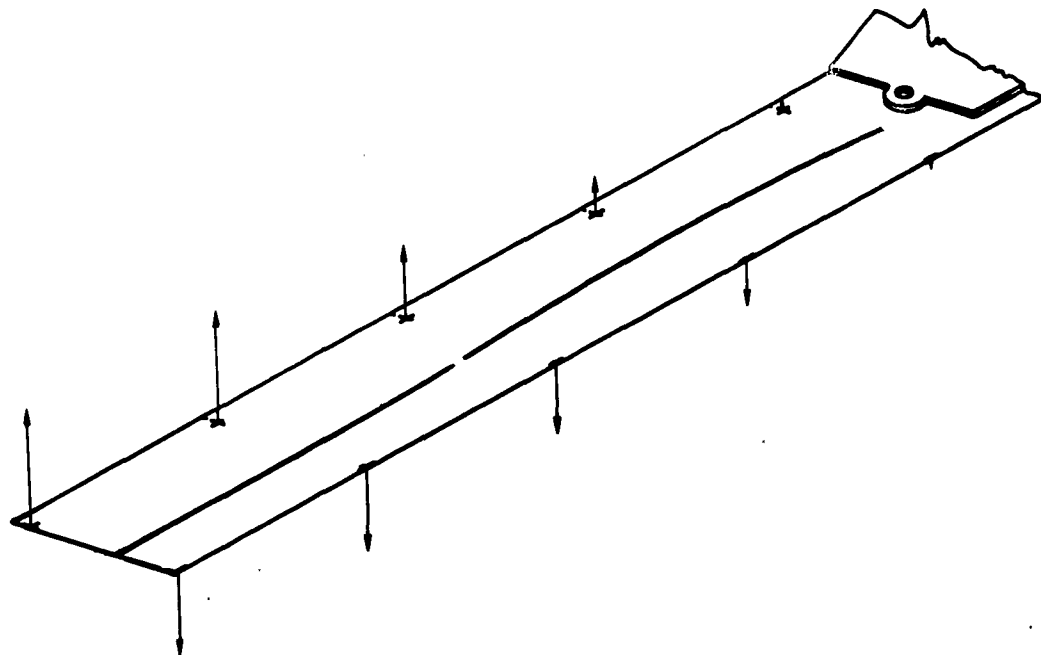Figure 52. Ground Vibration Test Mode Shape — Model S_3F_1, 85.5 cps, Damping Factor 0.002
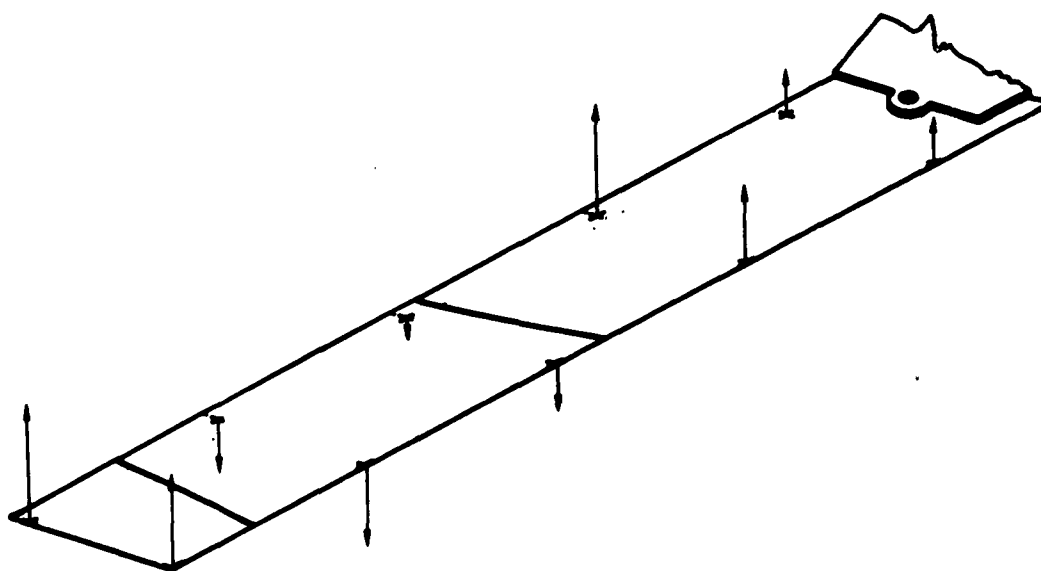
Figure 53. Ground Vibration Test Mode Shape — Model S_3F_1 118.0 cps, Damping Factor 0.024

4 | TOWING TANK TESTS

The test procedure used was similar to that used in flight flutter testing of aircraft. In general, the test specimen was accelerated to a test speed with the control in the deflected position, the control surface was released and the resulting foil response analyzed. Using this subcritical response, the next test configuration could be planned. The subcritical response of the surface did not prove satisfactory for predicting the onset of a flutter condition; however, the flutter response was a limited amplitude oscillation and allowed tests to be run at speeds in excess of the critical flutter speed without damage to the test specimen. The maximum speeds attainable were limited by divergence of the surface and wheel loads on the carriage. These limitations did not prevent obtaining flutter speeds for all configurations except the higher angles of attack and the deeper immersion depths.

No special tests were run on the dynamic characteristics of the carriage because of the exceedingly smooth running nature of the carriage. Figure 54 shows a plot of the vibratory accelerations and the frequency of the response of a beam in the center of the carriage. The primary source of excitation comes from the wheels which are nylon with rubber inserts. Nylon takes a temporary set if allowed to stand in one position for any length of time; however, several runs of the carriage rid the wheels of this set and do not provide any excitation which can be seen on the records. The lateral excitation is the primary forcing function (a maximum of ±0.0019 in. at 58 fps carriage speed) affecting the foil, and the foil response due to this generalized displacement was not apparent on the records.
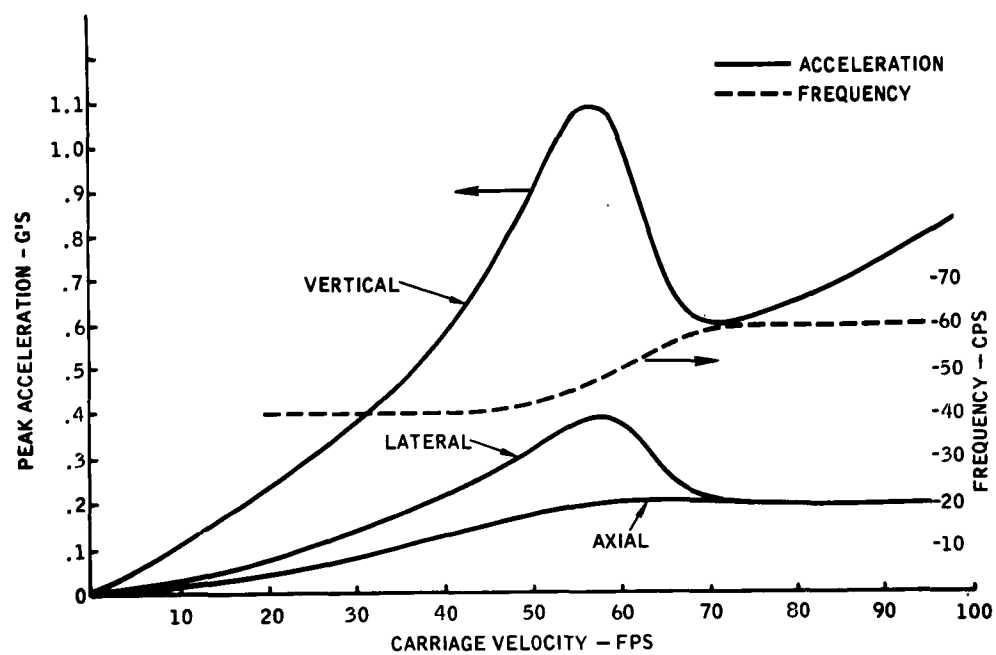
Figure 54. Carriage Response Versus Velocity
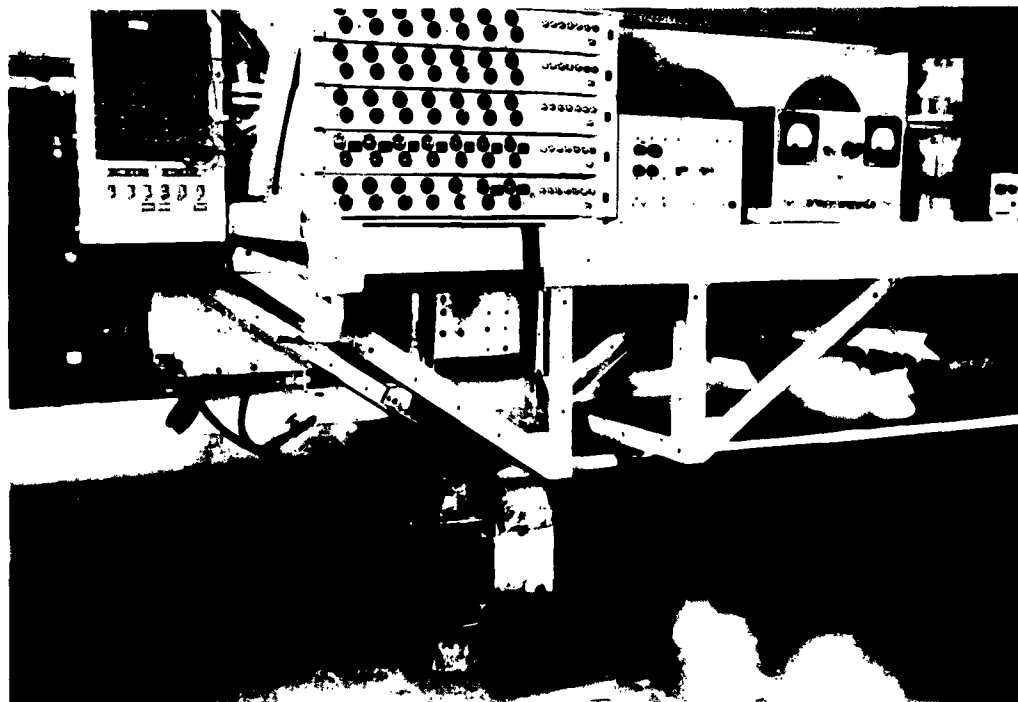
Figure 55. Telemetry Transmission Equipment

4.1 INSTRUMENTATION

The instrumentation installed on the foils consisted of strain gages oriented to measure:

a. Root bending moment,

b. Root torsion, and

c. Control surface deflection.

Pressure pickups were installed on the foils, but the pickup output proved noisy and time did not permit repair.

The strain gages were calibrated by applying known bending and torsion loads to the end of the foil. This provided the required calibration factors and allowed instrumentation gages to be calibrated for use in determining the approach to limit loads on the carriage wheels.

Because it was necessary to examine the records from the subcritical tests, the data was telemetered from the carriage (Figure 54) to a receiving station (Figure 55) where it was recorded on magnetic tape and a direct-writing oscillograph. Thus, the records could be analyzed almost immediately and also played back with filter characteristics as required.

Sixteen millimeter color motion pictures were taken of the foils at 64 fps. These pictures recorded the cavity size and location during the test. The camera location is shown in Figure 56. One difficulty encountered which could be attributed to the camera system consisted of a 60-cycle interference in the telemetry signal. This interference was due to the camera lights and appeared on all data traces the instant the lights came on. The interference did not affect the data but did require considerable diligence in reading the oscillograph records to insure that this interference was not confused with the foil response. This difficulty could have been rectified but would have required a major redesign of the telemetering system, which time did not permit.

41
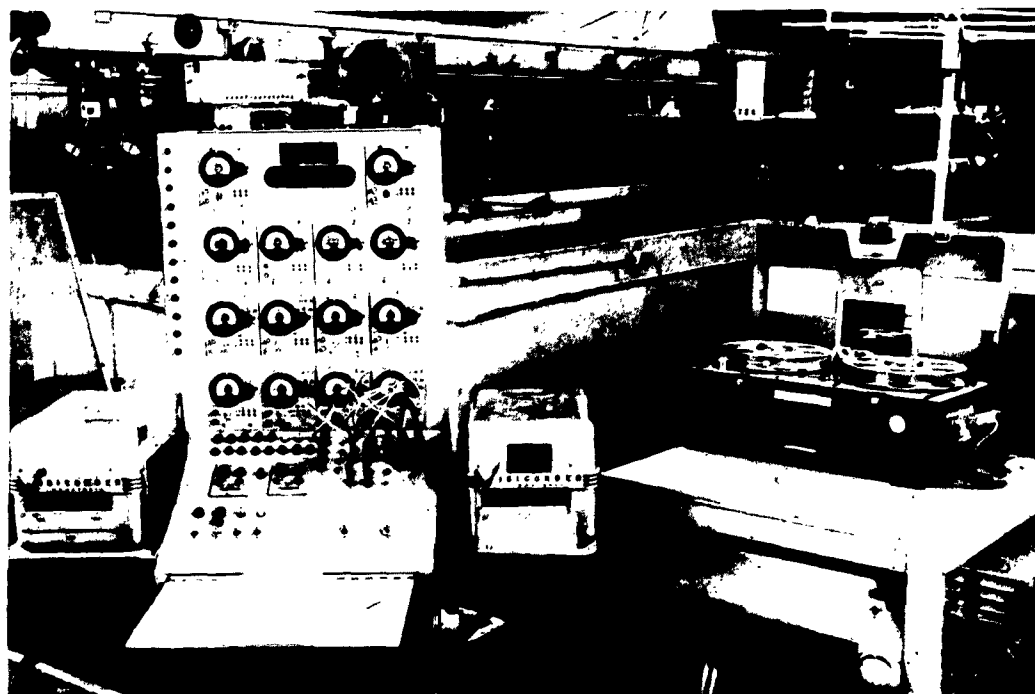
Figure 56. Telemetry Receiving Station
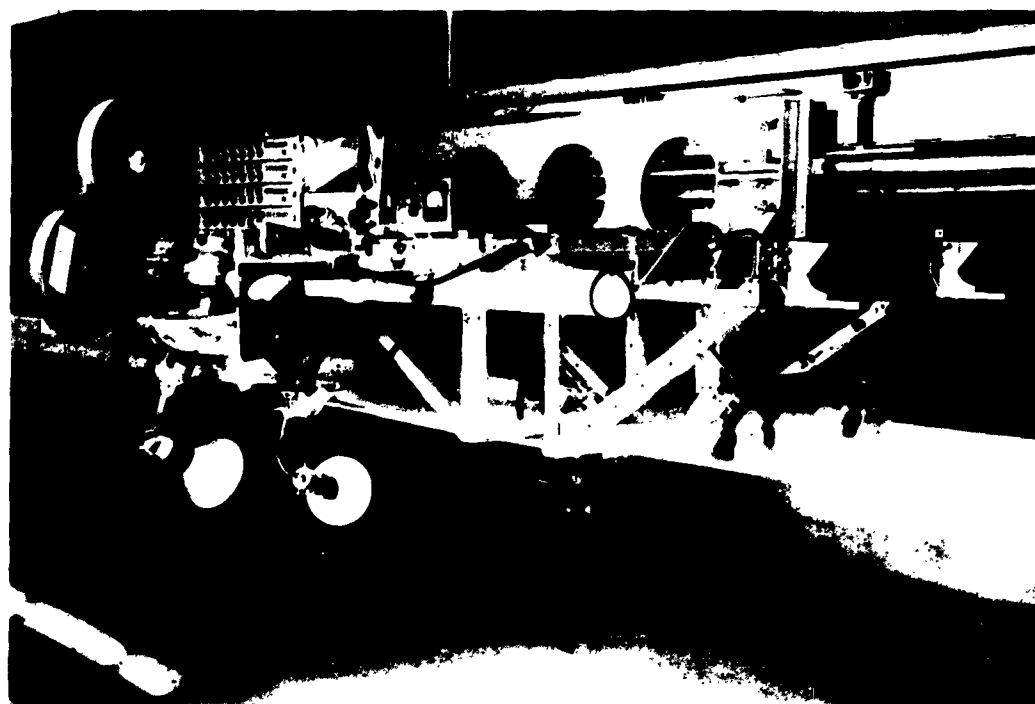
Figure 57. Camera Installation on Carriage

4.2 TEST PROCEDURE

The test configurations investigated included:

   a.   The effect of foil angle of attack from 0 to 4 deg.

   b.   The effect of the depth of immersion, 25, 50, 75, and 100 per cent.

   c.   The effect of control surface support stiffness, three stiffness rates.

   d.   Control surface chord —

      (1)   Rudder, 15, 25 and 35 per cent.

      (2)   Spoiler, 5, 7, and 10 per cent.

Initial tests were run to 80 fps in increments of approximately five feet per second. However, it was found that the flutter speeds fell below 50 fps and the system became more stable at the higher velocities. Thus, the later runs were limited to approximately 50 fps.

As runs were completed, a check was made on the approach to divergence which occurred once and the load on the carriage wheels which was a limiting condition. The nylon wheels provided a very smooth-running carriage but did limit the "rigid" body load which could be handled. This, of course, was most predominant at the higher angles of attack and the greater depths of immersion.

At speeds of 5 to 8 fps the foils were subject to a subcavitating limited-amplitude flutter. This flutter mode consisted of a predominantly foil-first bending mode with considerable coupling with a carriage rolling mode. Since the primary purpose of this investigation was concerned with supercavitating flutter, this condition was not studied other than to consider it in the test program. This flutter condition, which had to be traversed on each run, resulted in the early failure of the upper hinge point and introduced a permanent set in the lightest set of flexures of the spoiler models and one of the rudder models. Thus, all runs were made without the uppermost hinge point, and no runs were obtained with the lightest flexures of the spoiler models.

43

This procedure proved very satisfactory as a method for conducting tests of this type; however, if it or similar tests were to be run some of the revised procedures which would be used are as follows:

a. An automatic stopping device would be installed to brake the carriage to a stop when a preset foil load was obtained. Human reaction time is too long and too much margin must be allowed for equipment safety.

b. The telemetering system would be revised to use a separate power system to eliminate the 60-cycle interference caused by the camera lights.

c. Subcavitating flutter runs would be eliminated from the program to ease the fatigue problems introduced.

5 | RESULTS

The purpose of this test was to obtain the experimental flutter characteristics of a supercavitating hydrofoil with a control surface. No attempt is made to fix a theory to the data; rather, the data is presented just as obtained.

In general, the foil responses obtained resulted in two flutter speeds per configuration. Each flutter condition was a limited-amplitude sinusoidal oscillation. The control surface participated in each flutter mode and torsion was present in the flutter mode at 40 fps. Very little bending was noted in any supercavitating flutter mode.

Figures 58 to 71 show plots of the flutter-reduced frequency based on the torsional frequency of the foil in air from ground vibration test results versus the ratio of flutter frequency to torsional frequency. It should be noted that these flutter points are limit-cycle oscillations and do not result in failure of the foils. The speed may be increased to speeds above the flutter speed with increasing stability; however, prolonged running at the flutter speed may result in fatigue failure or difficulties affecting passenger comfort. Table 4 is a summary of the test data obtained.

During attempts at correlating this data it was found that, despite the configuration being tested, the flutter condition always fell at a $V/b\omega_f = 0.043$ or 0.086, where ω_f is the flutter frequency. The ratio of the flutter frequency to the torsional frequency in air fell between 0.4 and 0.6 with only an occasional point as low as 0.3 or as high as 0.7

The mass ratio, $\mu = m/\pi\rho b^2$, was equal to 0.34 and was not varied during the program.

45
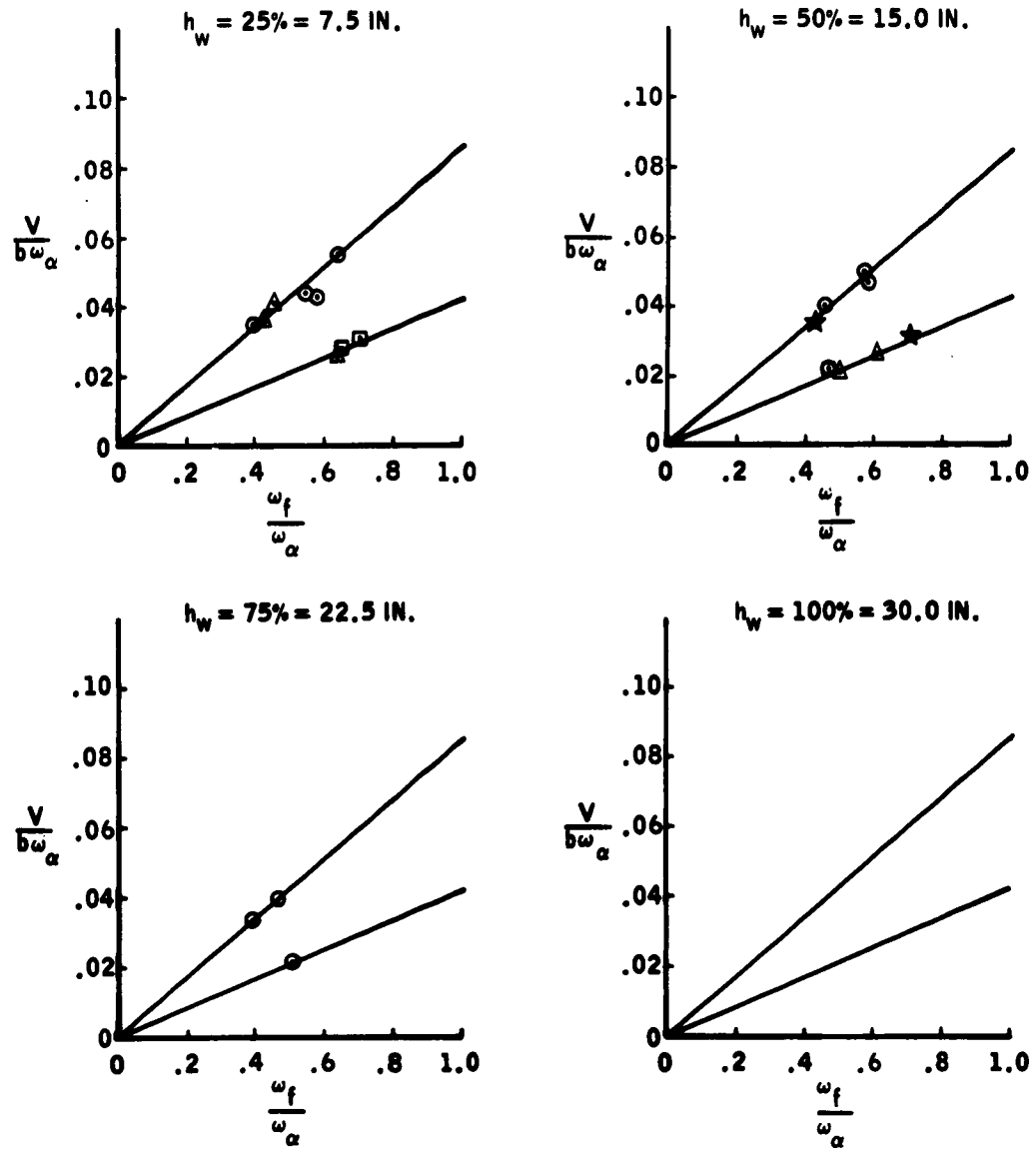
Figure 58. Supercavitating Hydrofoil Test Results,
Model Configuration R_1F_1

$$\Psi = \begin{cases} \bigcirc = 0^b \\ \star = 1^\circ \\ \triangle = 2^\circ \\ \square = 4^\circ \end{cases}$$

$h_w = 25\% = 7.5$ IN.

$h_w = 50\% = 15.0$ IN.

$\frac{V}{b\omega_\alpha}$

$\frac{\omega_f}{\omega_\alpha}$

$h_w = 75\% = 22.5$ IN.

$h_w = 100\% = 30.0$ IN.

$\frac{V}{b\omega_\alpha}$

$\frac{\omega_f}{\omega_\alpha}$
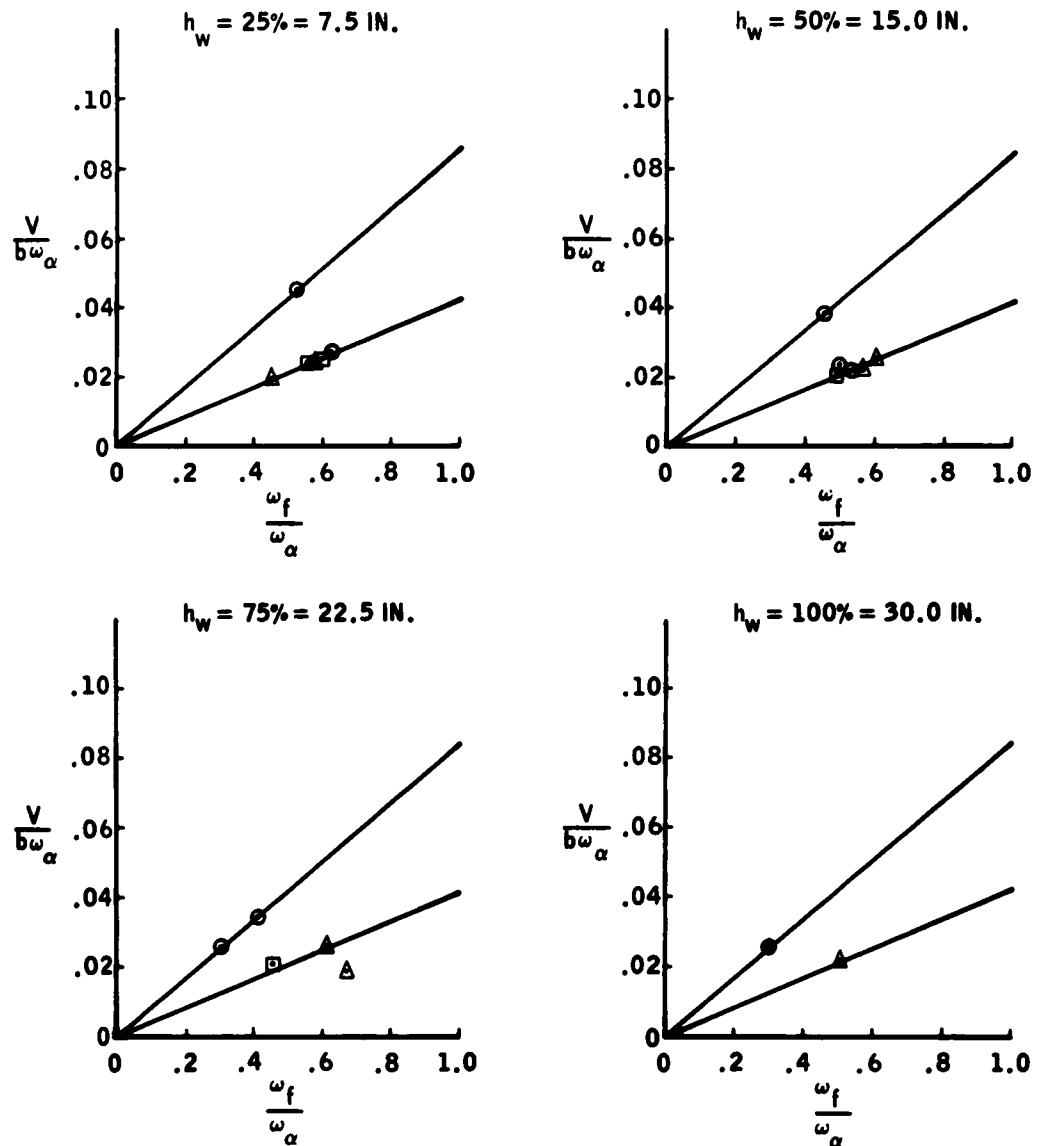
Figure 59. Supercavitating Hydrofoil Test Results,
Model Configuration $R_1 F_2$
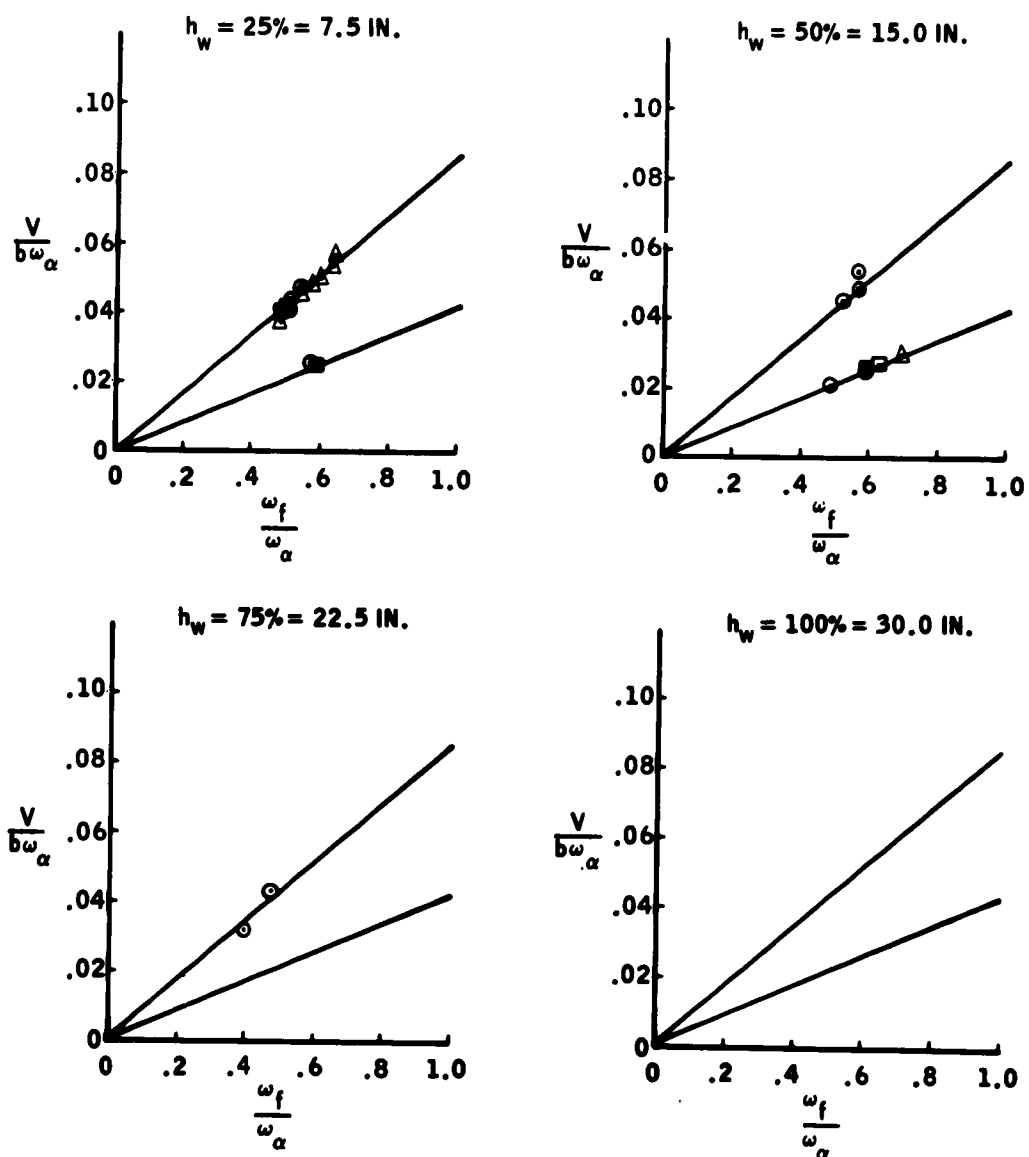
Figure 60. Supercavitating Hydrofoil Test Results,
Model Configuration R_2F_1
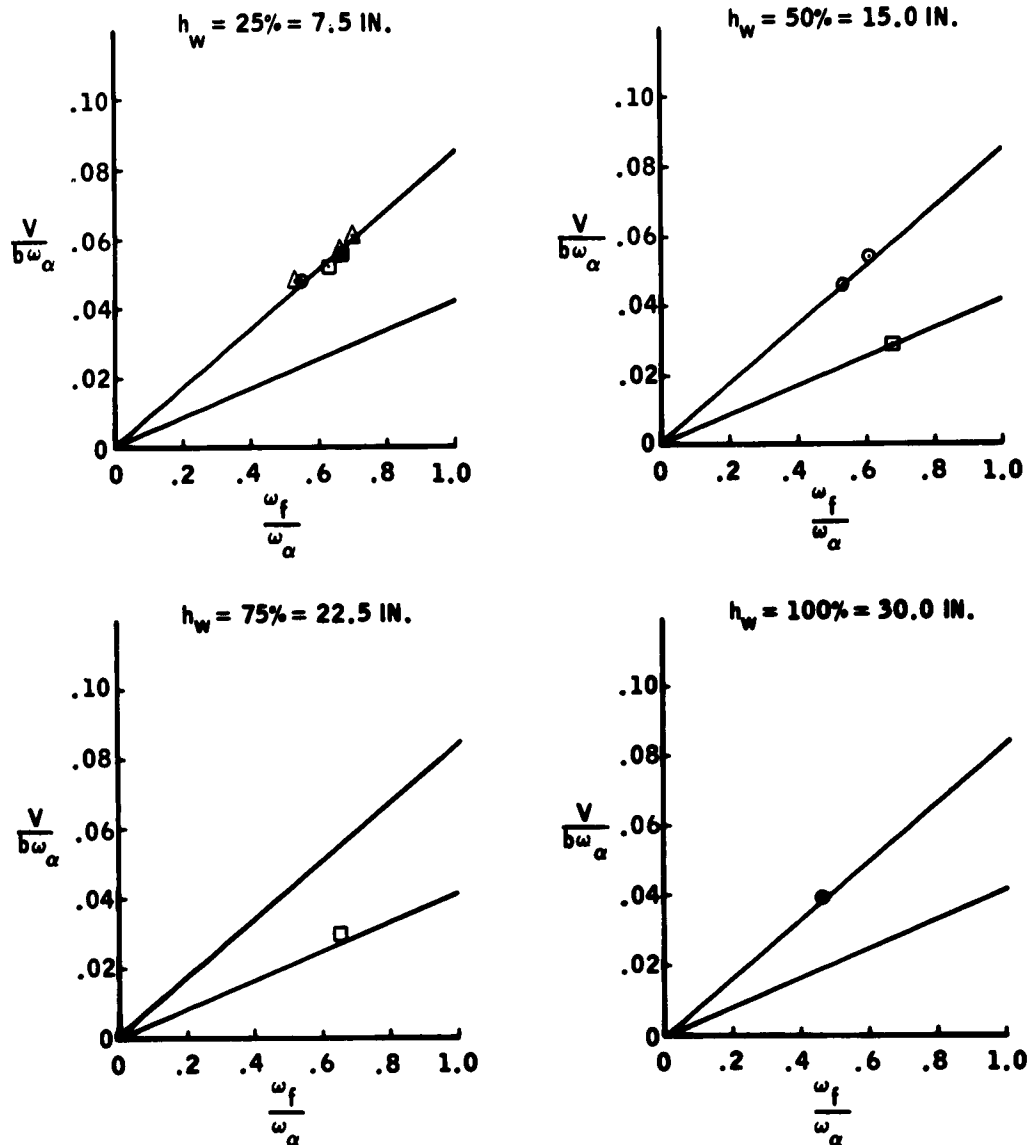
Figure 61. Supercavitating Hydrofoil Test Results,
Model Configuration $R_2 F_2$

49
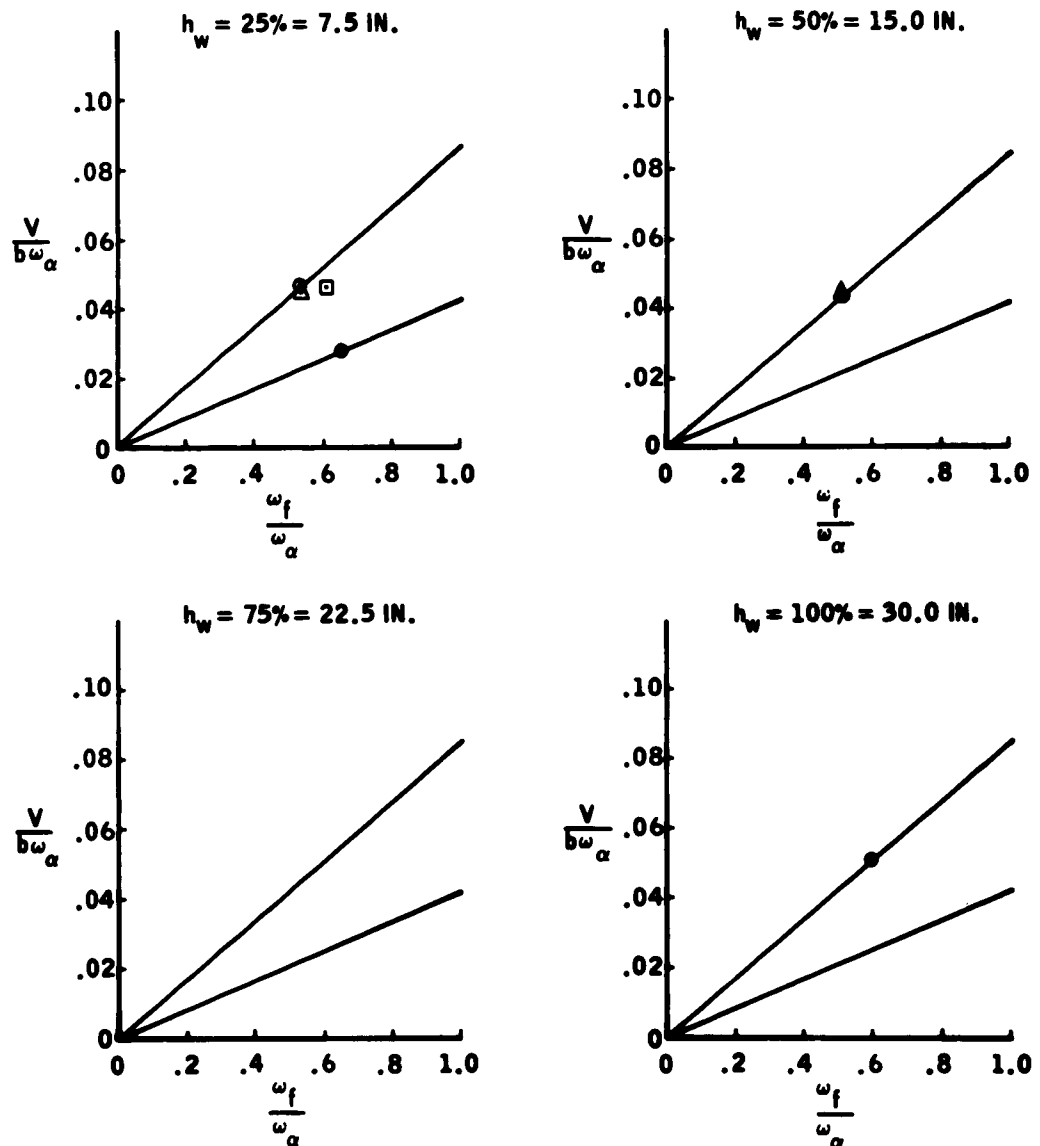
Figure 62. Supercavitating Hydrofoil Test Results,
Model Configuration R_2F_3
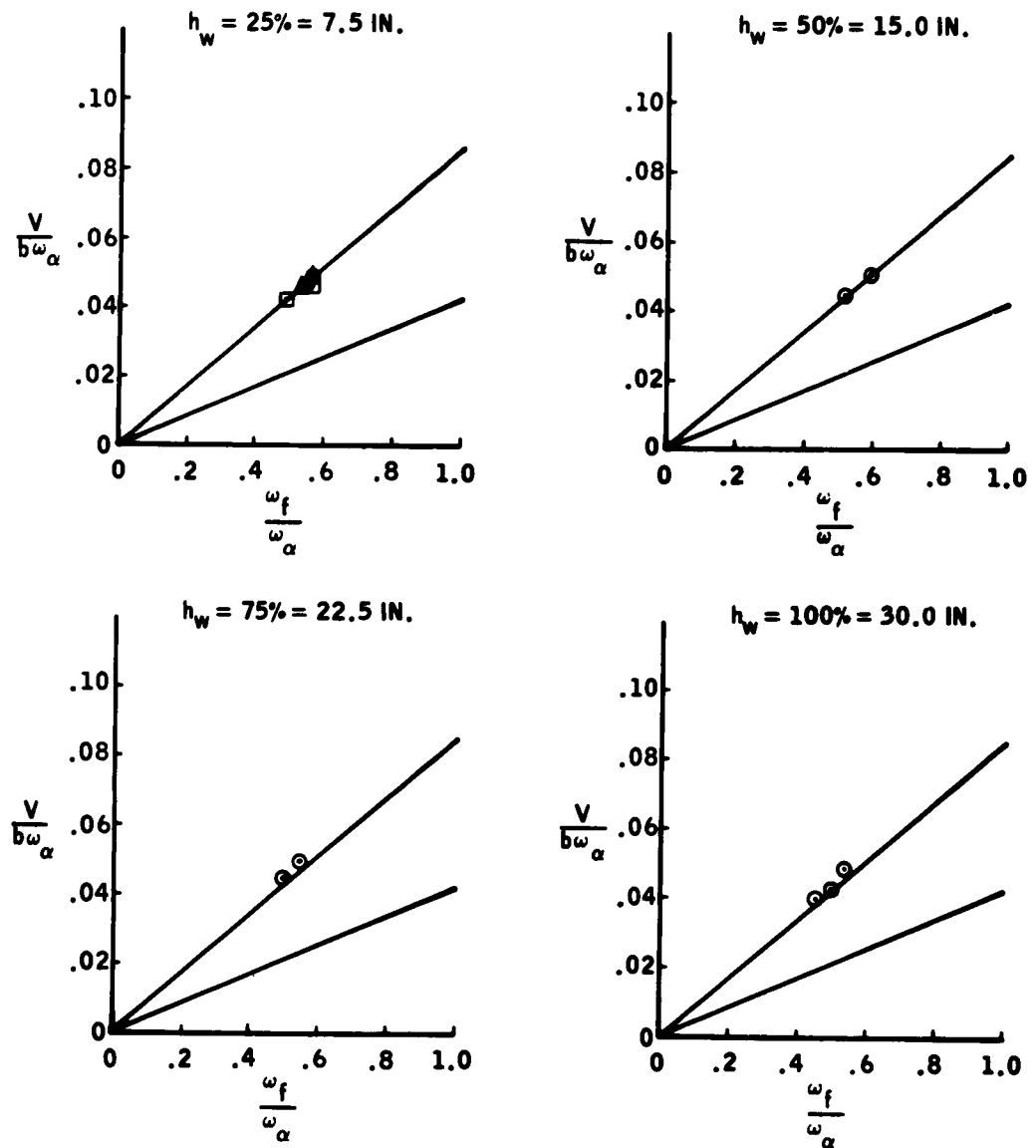
Figure 63.   Supercavitating Hydrofoil Test Results,
Model Configuration R_3F_1
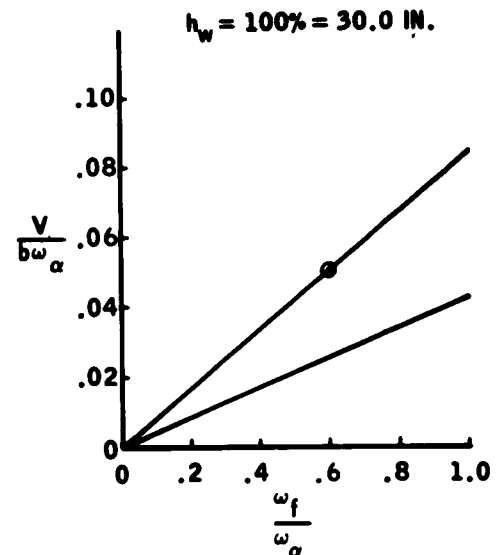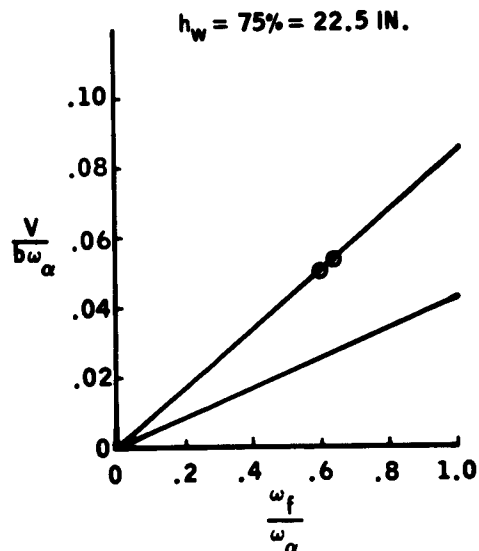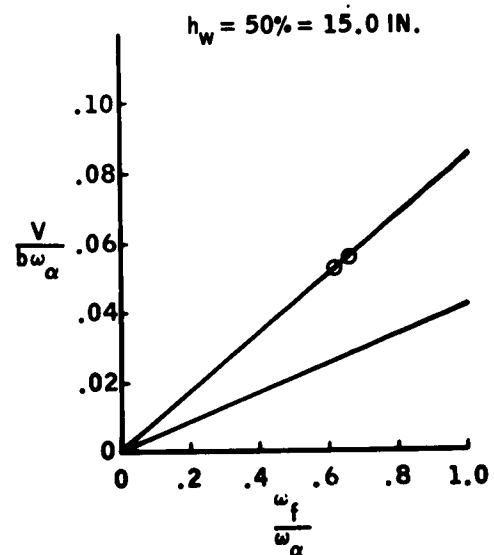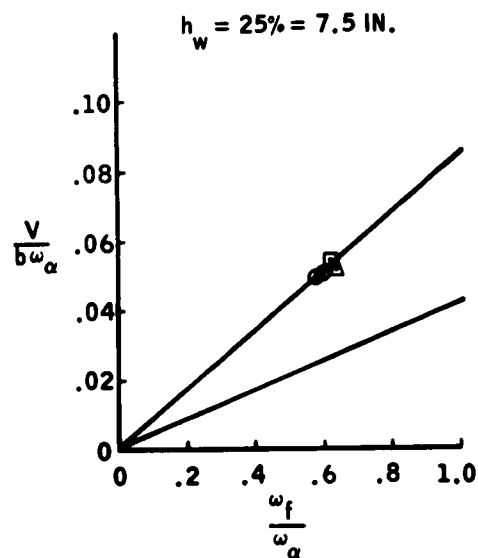
Figure 64. Supercavitating Hydrofoil Test Results,
Model Configuration R_3F_2
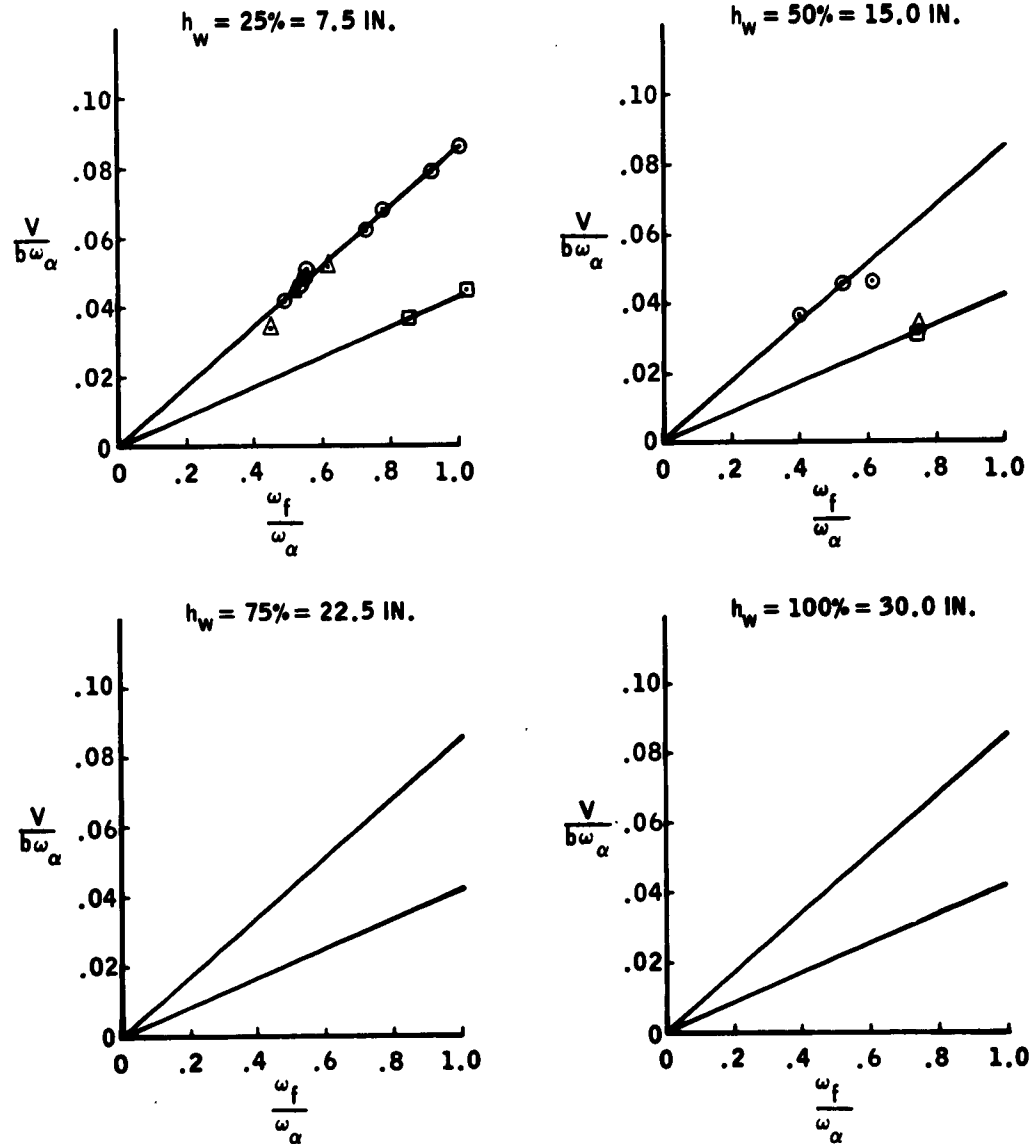
Figure 65. Supercavitating Hydrofoil Test Results,
Model Configuration R_3F_3
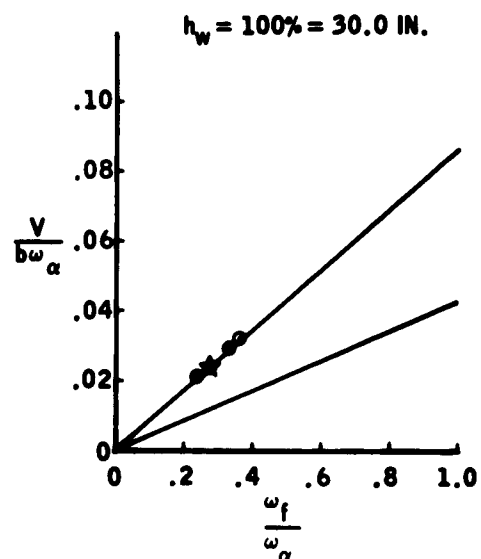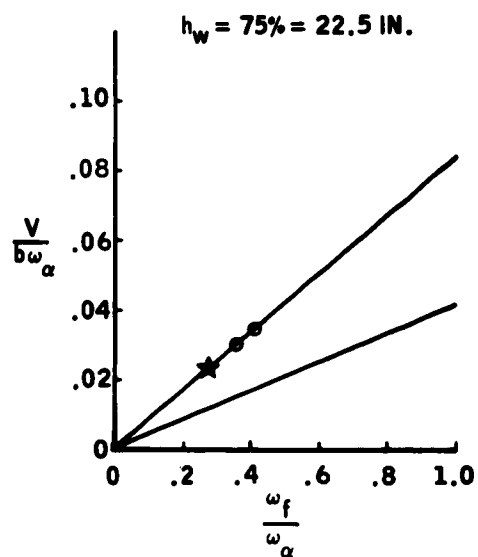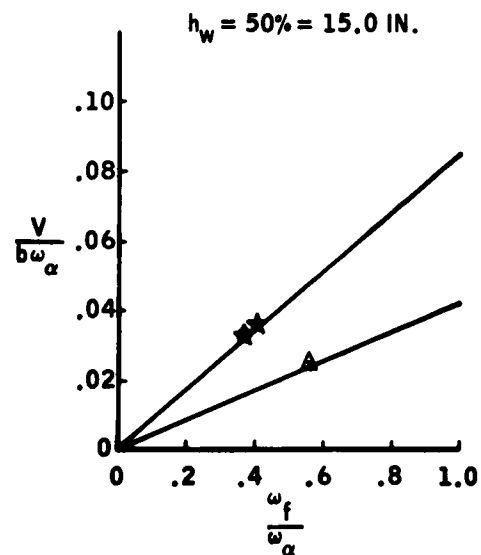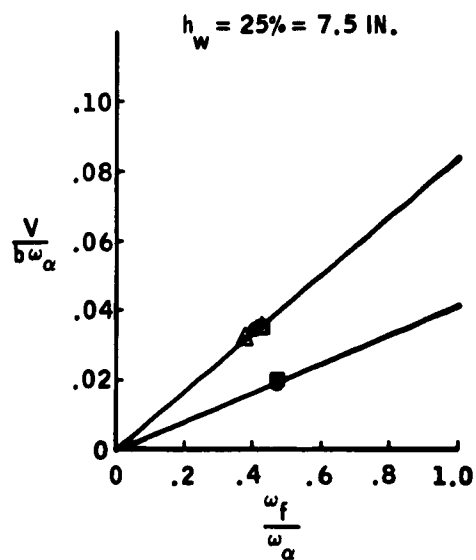
Figure 66. Supercavitating Hydrofoil Test Results,
Model Configuration $S_1 F_1$

54
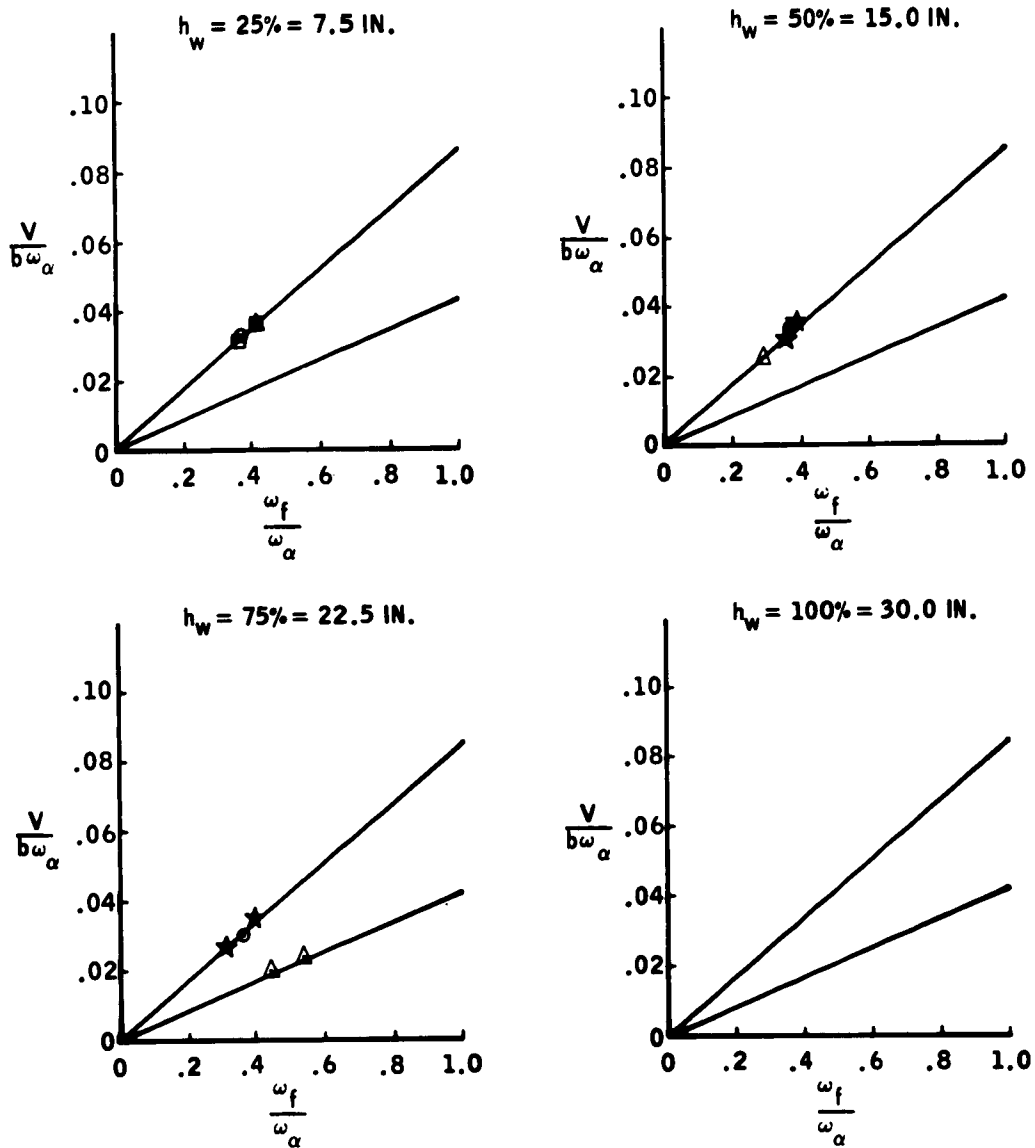
Figure 67. Supercavitating Hydrofoil Test Results,
Model Configuration $S_1 F_2$
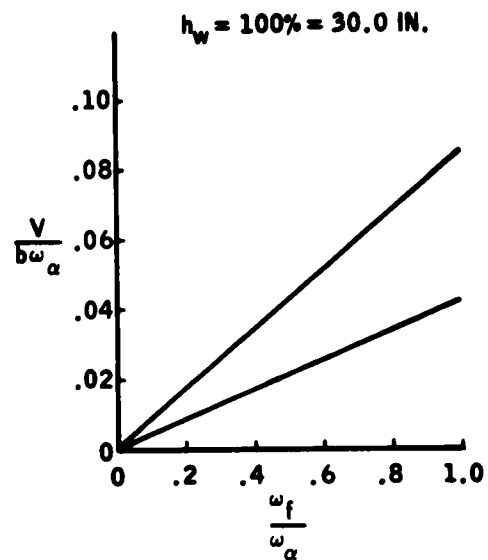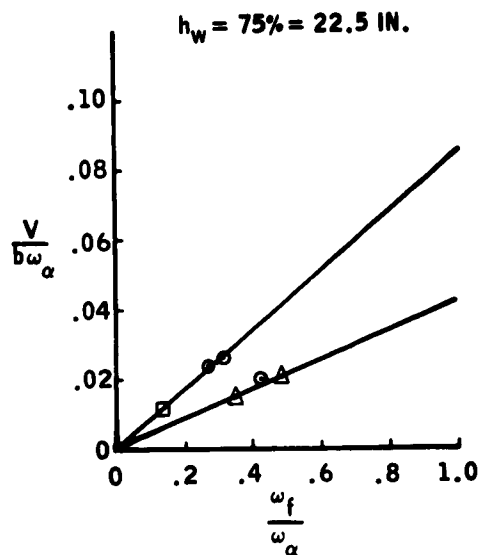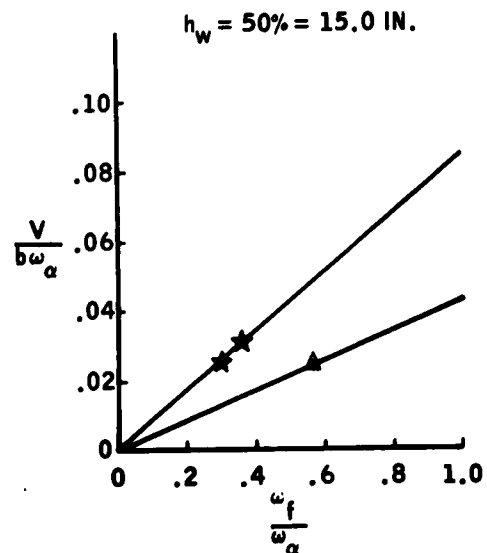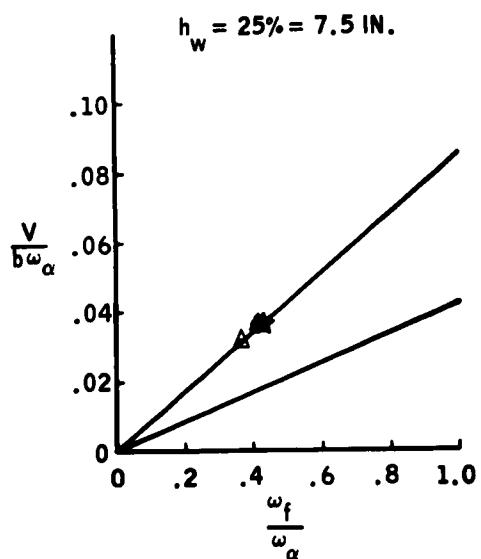
Figure 68. Supercavitating Hydrofoil Test Results,
Model Configuration S_2F_1
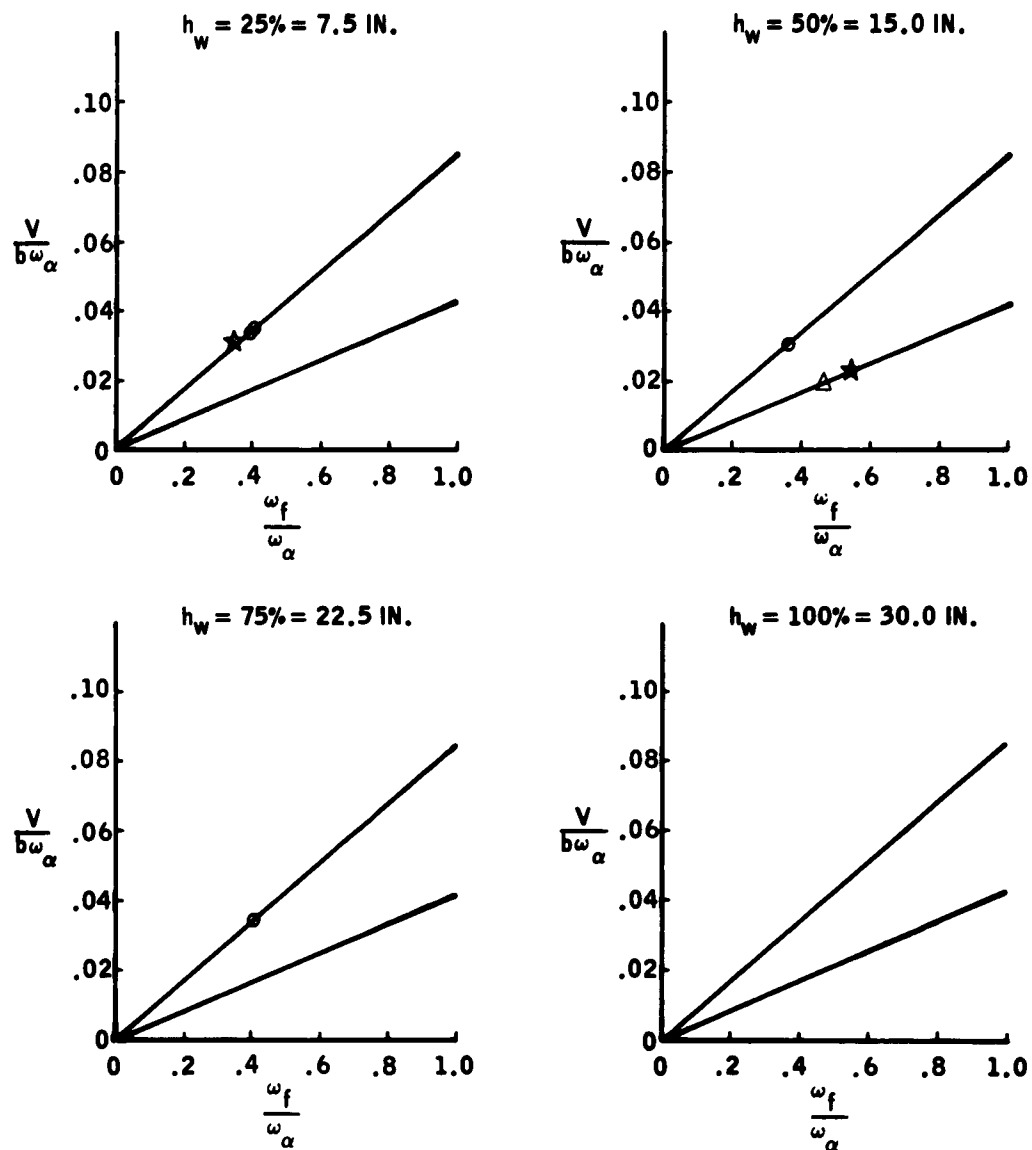
Figure 69. Supercavitating Hydrofoil Test Results,
Model Configuration $S_2 F_2$
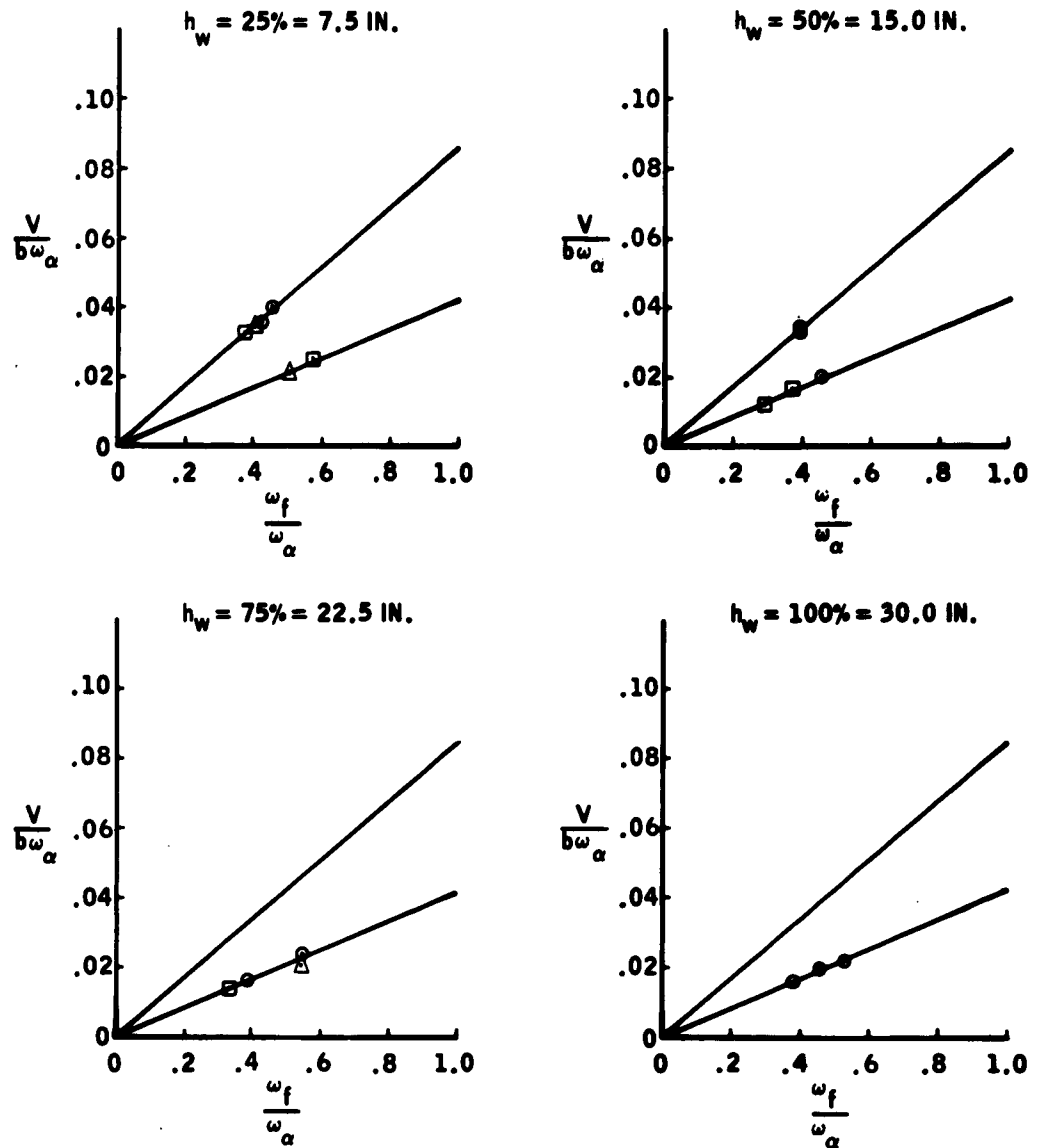
Figure 70. Supercavitating Hydrofoil Test Results,
Model Configuration S_3F_1
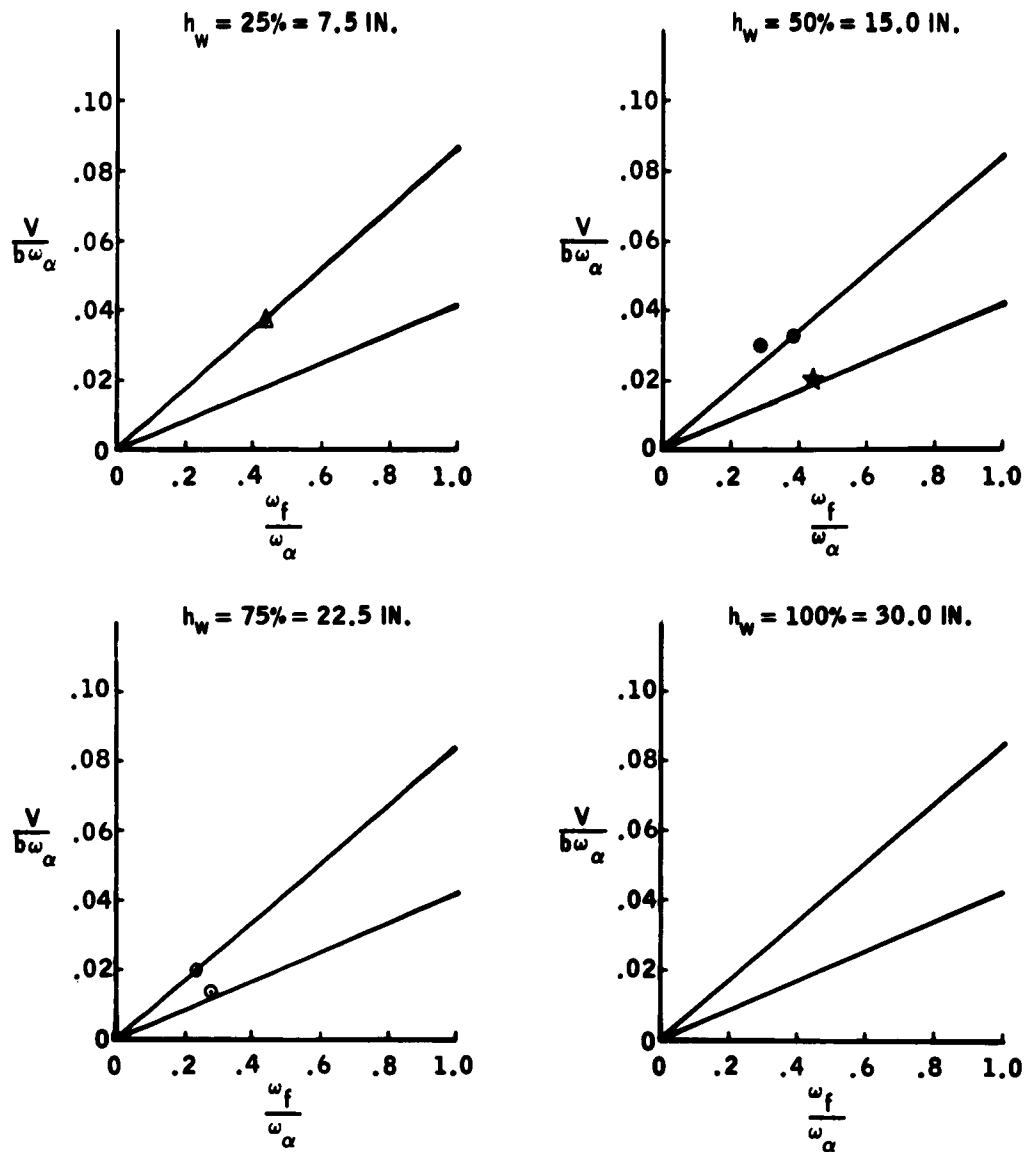
Figure 71.   Supercavitating Hydrofoil Test Results,
Model Configuration S_3F_2

59

Table 4. Summary of Test Results

Configuration		f_α cps	h_w in.	ψ deg.	V_f ft/sec	f_f cps	$\dfrac{f_f}{f_\alpha}$	$\dfrac{V_f}{b\omega_f}$	$\dfrac{V_f}{b\omega_\alpha}$
R_1	F_1	77.8	7.5	0	39	31	.398	.088	.035
					48	38	.488	.088	.043
					51	42	.540	.085	.044
					62	49	.630	.089	.055
				2	29	48	.617	.042	.026
					40	32	.411	.088	.036
					45	35	.450	.090	.041
				4	31	50	.640	.043	.028
					34	54	.695	.044	.031
			15	0	24	36	.463	.047	.022
					52	45	.579	.081	.047
					55	44	.566	.087	.050
					39	33	.424	.083	.035
					44	35	.450	.088	.040
				1	34	55	.706	.043	.031
					39	33	.424	.083	.035
				2	23	39	.501	.041	.021
					29	47	.604	.043	.026
				4	24	36	.463	.047	.022
			22.5	0	24	39	.501	.043	.022
					38	31	.398	.086	.034
					45	36	.463	.087	.040
R_1	F_2	73.2	7.5	0	28	45	.616	.043	.027
					47	81	.520	.086	.045
				2	25	42	.575	.042	.024
					21	33	.451	.045	.020

60

Table 4. Summary of Test Results (Continued)

Configuration		f_α cps	h_w in.	ψ deg.	V_f ft/sec	f_f cps	$\dfrac{f_f}{f_\alpha}$	$\dfrac{V_f}{b\omega_f}$	$\dfrac{V_f}{b\omega_\alpha}$
R_1	F_2	73.2	7.5	4	25	40	.549	.044	.024
					26	43	.589	.042	.025
			15	0	23	39	.534	.041	.022
					25	36	.494	.048	.024
					41	33	.451	.087	.039
				2	24	41	.561	.041	.023
					27	44	.602	.041	.026
				4	22	35	.480	.044	.021
			22.5	0	37	30	.410	.086	.035
					27	22	.300	.086	.026
				2	27	44	.602	.043	.026
				4	22	33	.451	.047	.021
			30	0	27	22	.300	.086	.026
				2	23	37	.506	.044	.022
R_2	F_1	67.6	7.5	0	25	38	.563	.046	.026
					41	34	.503	.085	.042
					42	34	.503	.086	.044
					46	36	.533	.089	.048
				2	37	32	.473	.081	.038
					40	32	.473	.087	.041
					44	36	.532	.086	.046
					46	38	.560	.085	.048
					48	40	.590	.084	.050
					52	42	.622	.086	.054

Table 4. Summary of Test Results (Continued)

Configuration		f_α cps	h_w in.	ψ deg.	V_f ft/sec	f_f cps	$\dfrac{f_f}{f_\alpha}$	$\dfrac{V_f}{b\omega_f}$	$\dfrac{V_f}{b\omega_\alpha}$
↓	↓	↓	↓	↓	55	43	.638	.089	.057
				4	24	39	.580	.043	.025
				↓	40	32	.474	.087	.041
↓	↓	↓	↓	↓	41	33	.489	.087	.042
R_2	F_1	67.6	15	0	20	33	.489	.042	.021
				↓	23	40	.592	.042	.025
					43	35	.519	.086	.045
					47	38	.562	.086	.049
				↓	52	38	.562	.096	.054
				2	29	47	.696	.058	.030
				4	25	40	.592	.043	.026
			↓	↓	26	42	.622	.043	.027
			22.5	0	31	27	.400	.080	.032
↓	↓	↓	↓	↓	41	32	.473	.090	.043
R_2	F_2	58.8	7.5	0	40	33	.543	.086	.048
				2	40	33	.543	.086	.048
					48	39	.664	.086	.057
				↓	51	41	.697	.087	.061
				4	44	37	.630	.083	.052
			↓	↓	47	39	.664	.084	.056
			15	0	39	32	.534	.085	.046
			↓	↓	45	36	.611	.087	.054
			↓	4	24	40	.680	.042	.029
			22.5	4	25	38	.646	.046	.030
↓	↓	↓	30	0	34	27	.459	.088	.040

Table 4. Summary of Test Results (Continued)

Configuration		f_α cps	h_w in.	ψ deg.	V_f ft/sec	f_f cps	$\dfrac{f_f}{f_\alpha}$	$\dfrac{V_f}{b\omega_f}$	$\dfrac{V_f}{b\omega_\alpha}$
R_2	F_3	60.0	7.5	0	24	39	.650	.043	.028
				↓	40	32	.534	.087	.047
				2	39	32	.534	.086	.045
			↓	4	40	36	.600	.078	.046
			15	0	38	31	.517	.086	.044
			↓	2	39	31	.517	.088	.045
			30	0	45	36	.600	.087	.052
R_3	F_1	60.4	7.5	0	40	33	.546	.085	.046
				↓	42	34	.564	.086	.049
				2	39	32	.530	.086	.045
				↓	42	34	.564	.086	.049
				4	36	30	.496	.084	.042
			↓	↓	40	33	.546	.085	.046
			15	0	39	31	.514	.088	.045
			↓	↓	44	36	.596	.086	.051
			22.5	0	39	30	.496	.091	.045
			↓	↓	43	33	.546	.091	.050
			30	0	35	27	.447	.091	.040
				↓	37	30	.496	.086	.043
			↓	↓	42	32	.530	.092	.049
R_3	F_2	52.0	7.5	0	36	30	.576	.084	.049
				↓	37	31	.596	.084	.050
				2	39	33	.635	.083	.052
			↓	4	40	32	.615	.088	.054
			15	0	39	32	.615	.085	.052
			↓	↓	42	34	.655	.086	.056

63

Table 4. Summary of Test Results (Continued)

Configuration		f_α cps	h_w in.	ψ deg.	V_f ft/sec	f_f cps	$\dfrac{f_f}{f_\alpha}$	$\dfrac{V_f}{b\omega_f}$	$\dfrac{V_f}{b\omega_\alpha}$
			22.5	0	38	31	.596	.086	.051
			↓	↓	40	33	.635	.085	.054
↓	↓	↓	30	0	38	31	.596	.086	.051
R₃	F₃	47.0	7.5	0	28	23	.489	.085	.042
					31	25	.532	.087	.046
					32	26	.553	.086	.048
					34	26	.553	.091	.051
					42	34	.723	.086	.062
					46	37	.787	.087	.068
					53	43	.915	.086	.079
↓	↓	↓	↓	↓	58	47	1.000	.086	.086
R₃	F₃	47.0	7.5	2	23	21	.446	.077	.034
					30	25	.532	.084	.045
				↓	35	29	.616	.085	.052
				4	25	40	.851	.044	.037
			↓	↓	30	48	1.020	.044	.045
			15	0	24	19	.404	.088	.036
					30	25	.532	.084	.045
				↓	31	29	.616	.075	.046
				2	22	35	.744	.044	.033
↓	↓	↓	↓	4	21	35	.744	.042	.031
S₁	F₁	85.3	7.5	0	24	40	.469	.040	.020
				↓	44	35	.410	.088	.036
				2	40	32	.375	.087	.033
				↓	44	36	.422	.086	.036
↓	↓	↓	↓	4	25	40	.469	.044	.021

Table 4. Summary of Test Results (Continued)

Configuration	f_α cps	h_w in.	ψ deg.	V_f ft/sec	f_f cps	$\dfrac{f_f}{f_\alpha}$	$\dfrac{V_f}{b\omega_f}$	$\dfrac{V_f}{b\omega_\alpha}$
		↓	↓	44	36	.422	.086	.036
		15	0	40	32	.375	.087	.033
		↓	1	39	32	.375	.085	.032
			↓	44	35	.410	.088	.036
		↓	2	30	48	.561	.044	.025
		22.5	0	38	31	.363	.086	.031
			↓	43	35	.410	.086	.035
		↓	1	29	24	.278	.085	.024
		30	0	25	20	.235	.088	.021
				29	24	.278	.085	.024
				35	28	.328	.088	.029
			↓	39	31	.363	.088	.032
		↓	1	29	24	.278	.085	.024
S_1	F_2 85.3	7.5	0	40	32	.375	.087	.033
			↓	44	36	.422	.086	.036
			2	44	36	.422	.086	.036
			4	38	31	.363	.086	.031
		↓	↓	44	36	.422	.086	.036
		.15	0	38	31	.363	.086	.031
			↓	41	32	.375	.089	.034
			1	38	31	.363	.086	.031
			↓	43	33	.387	.091	.035
		↓	2	30	25	.293	.084	.025
		22.5	0	33	27	.316	.086	.027
		↓	↓	36	31	.363	.081	.030
↓	↓	↓	1	33	27	.316	.086	.027

Table 4. Summary of Test Results (Continued)

Configuration		f_α cps	h_w in.	ψ deg.	V_f ft/sec	f_f cps	$\dfrac{f_f}{f_\alpha}$	$\dfrac{V_f}{b\omega_f}$	$\dfrac{V_f}{b\omega_\alpha}$
				↓	43	34	.398	.089	.035
				2	24	38	.445	.044	.020
				↓	29	46	.540	.044	.024
S_2	F_1	85.4	7.5	0	44	35	.410	.088	.036
				1	44	36	.422	.086	.036
				2	39	31	.363	.088	.032
				↓	44	35	.410	.088	.036
			15	1	30	26	.305	.081	.025
				↓	38	31	.364	.086	.031
				2	30	48	.564	.044	.025
			22.5	0	24	36	.422	.047	.020
					29	23	.270	.088	.024
				↓	32	27	.317	.083	.026
				2	19	30	.352	.044	.015
				↓	25	41	.481	.043	.021
				4	15	12	.141	.087	.012
S_2	F_1	85.4	30	0	27	22	.258	.086	.022
				4	15	22	.258	.048	.012
S_2	F_2	85.3	7.5	0	41	34	.400	.084	.034
				↓	42	35	.410	.084	.035
				1	38	30	.352	.088	.031
				2	38	30	.352	.088	.031
			15	0	38	31	.364	.086	.031
				1	28	46	.540	.043	.023
				2	24	40	.470	.042	.020
			22.5	0	43	35	4.10	.086	.035

Table 4. Summary of Test Results (Continued)

Configuration		f_α cps	h_w in.	ψ deg.	V_f ft/sec	f_f cps	$\dfrac{f_f}{f_\alpha}$	$\dfrac{V_f}{b\omega_f}$	$\dfrac{V_f}{b\omega_\alpha}$
S_3	F_1	85.5	7.5	0	44	36	.422	.086	.036
				↓	49	39	.458	.088	.040
				2	26	43	.504	.042	.021
					41	35	.410	.082	.034
				↓	42	35	.410	.084	.035
				4	30	49	.575	.043	.025
			↓	↓	40	32	.375	.087	.033
			15	0	42	34	.398	.086	.034
				↓	40	34	.398	.082	.033
				2	24	39	.457	.043	.020
				4	15	25	.293	.042	.012
			↓	↓	20	32	.375	.044	.016
			22.5	0	20	33	.387	.042	.016
				↓	29	47	.550	.043	.024
				2	25	38	.446	.046	.021
				4	17	28	.328	.043	.014
			30	0	24	39	.457	.043	.020
				↓	20	33	.387	.042	.016
		↓	↓	↓	27	45	.527	.042	.022
S_3	F_2	85.5	7.5	2	45	37	.434	.085	.037
			15	0	36	27	.293	.100	.030
				↓	40	33	.387	.085	.033
			↓	1	24	38	.445	.044	.020
			22.5	0	24	20	.235	.084	.020
		↓	↓	↓	29	24	.282	.085	.024

6 | RECOMMENDATIONS

The results of this testing on a supercavitating hydrofoil show that flutter could be a serious problem with surface-piercing supercavitating hydrofoils, especially from the fatigue and comfort standpoint. At the Fourth Symposium on Naval Hydrodynamics held in Washington, D. C., August 27 - 31, 1962, an ad-hoc committee on this subject heard that work in the Netherlands showed that sweep could have a marked effect on the flutter stability of hydrofoils. In these tests, flutter speeds were reduced below those found for zero sweep until a sweep angle of about ten degrees was attained. It would, therefore, be imperative that the flutter characteristics of the supercavitating hydrofoil under swept conditions be investigated.

The results could also be used to investigate the validity of theoretical analyses of this type of foil.

DISTRIBUTION LIST FOR FINAL REPORT
UNDER CONTRACT NObs-86810

No. of Copies

7	Chief, Bureau of Ships Washington 25, D. C. 3 Technical Library (Code 210L) 1 Ships Research (Code 340) 1 Preliminary Design (Code 421) 2 Hull Design (Code 442)
9	Commanding Officer and Director David Taylor Model Basin Washington 7, D. C.
1	Chief of Naval Research Fluid Dynamics Branch (Code 438) Department of the Navy Washington 25, D. C.
1	National Bureau of Standards Washington 25, D. C. (1) Dr. G. B. Schubauer, Chief Fluid Mechanics Section
1	Director Langley Research Center Langley Field, Virginia
1	National Research Council of Canada Hydromechanics Laboratory Ottawa 2, Canada
1	Office of Research & Development Maritime Administration 441 G Street, N. W. Washington 25, D. C.
10	Defense Documentation Center Headquarters Cameron Station Alexandria, Virginia

1   Office of Technical Services
       OTS, Department of Commerce
       Washington 25, D. C.

1   Commander
       Air Research & Development Command
       Attention: Mechanics Branch
       Air Force Office of Scientific Research
       14th and Constitution
       Washington 25, D. C.

1   Commander
       Wright Air Development Division
       Aircraft Laboratory
       Attention: Mr. W. Mykytow, Dynamics Branch
       Wright-Patterson Air Force Base, Ohio

1   National Physical Laboratory, Ship Division
       Teddington, Middlesex, England

1   Head, Aerodynamics Department
       Royal Aircraft Establishment
       Mr. M. C. W. Wolfe
       Farnborough, Hants, England

1   Boeing Airplane Co., Seattle Division
       Mr. M. J. Turner
       Seattle, Washington

3   California Institute of Technology
       Pasadena, California
         (1) Dr. M. S. Plesset
         (1) Dr. T. Y. Wu
         (1) Dr. A. J. Acosta

1   Cornell Aeronautical Laboratory
       4455 Genesee Street
       Buffalo, New York

2   Director, Davidson Laboratory
    Stevens Institute of Technology
    Hoboken, New Jersey
        (1) Mr. C. J. Henry
        (1) Mr. S. Tsakonas

1   Electric Boat Division
    General Dynamics Corp.
    Attention: Mr. Robert McCandliss
    Groton, Connecticut

1   General Applied Sciences Laboratories, Inc.
    Attention: Dr. F. Lane
    Merrick and Stewart Avenues
    Westbury, Long Island, New York

1   Gibbs and Cox, Inc.
    21 West Street
    New York, New York

2   Grumman Aircraft Engineering Corp.
    Bethpage, Long Island, New York
        (1) Mr. E. Baird
        (1) Mr. E. Bower

2   President, Hydronautics, Inc.
    Laurel, Maryland

1   Lockheed Aircraft Corp.
    Missiles and Space Division
    Attention: R. W. Kermeen
    Palo Alto, California

3   Massachusetts Institute of Technology
    Fluid Dynamics Research Laboratory
    Cambridge 39, Massachusetts
        (1) Prof. H. Ashley
        (1) Prof. M. Landahl
        (1) Prof. J. Dugundji

2	Director, Dept. of Mechanical Sciences
	Southwest Research Institute
	8500 Culebra Road
	San Antonio 6, Texas
	    (1) Dr. N. H. Abramson
	    (1) Editor, Applied Mechanics Review

1	Stanford University Department of Mathematics Stanford, California
1	State University of Iowa Iowa Institute of Hydraulic Research Prof. L. Landweber Iowa City, Iowa
1	Technical Research Group, Inc. Attention: Dr. J. Kotik 2 Aerial Way Syosset, Long Island, New York
1	University of California Department of Engineering Institute of Engineering Research Attention: Dr. J. V. Wehausen Berkeley, California
1	St. Anthony Falls Hydraulic Laboratory University of Minnesota Minneapolis, Minnesota
1	Oceanics, Inc. Technical Industrial Park Plainview, Long Island, New York

C-2347 (75)